ABSTRACT

Title of Thesis: MODELING IMPACTS OF SUBMERSED AQUATIC VEGETATION ON SEDIMENT DYNAMICS UNDER STORM CONDITIONS IN UPPER CHESAPEAKE BAY

Mathew Michael Biddle, Master of Science, 2019

Thesis directed by: Dr. Lawrence Sanford, UMCES
Dr. Cindy Palinkas, UMCES

Submersed aquatic vegetation is an important modulator of sediment delivery from the Susquehanna River through the Susquehanna Flats into the Chesapeake Bay. However, the impact of vegetation coupled with the physical drivers of sediment transport through the region are not well understood. This study used a new vegetation component in a coupled flow-wave-sediment transport modeling system (COAWST) to simulate summer through fall 2011, when the region experienced a sequence of events including Hurricane Irene and Tropical Storm Lee. Fine sediment was exported under normal flows and high wind forcing but accumulated under high flows. The relative effect of vegetation under normal and high wind forcing depended on previous sediment dynamics. Vegetation doubled the accumulation of fine sediments under high flows. While further refinement of the bed model may be needed to capture some nuances, the COAWST modeling system provides new insights into detailed sediment dynamics in complex vegetated deltaic systems.

MODELING IMPACTS OF SUBMERSED AQUATIC VEGETATION ON SEDIMENT DYNAMICS UNDER STORM CONDITIONS IN UPPER CHESAPEAKE BAY

by

Mathew Michael Biddle

Thesis submitted to the Faculty of the Graduate School of the
University of Maryland, College Park, in partial fulfillment
of the requirements for the degree of
Master of Science
2019

Advisory Committee:

Dr. Cindy Palinkas, Co-Chair
Dr. Lawrence Sanford, Co-Chair
Dr. Karen Prestegaard

Foreword

All of the specific configuration files for the COAWST modeling system used in this study are available via https://zenodo.org/record/3537968#.XeaHoZNKiL4 (DOI: 10.5281/zenodo.3537968). This repository includes the various start-up scripts for each model subcomponent as well as the input data for model forcing. The specific version of COAWST used for this study was r1393 last revised on 2019-02-11.

Acknowledgements

I would like to thank my academic advisors, Dr. Cindy Palinkas and Dr. Lawrence Sanford, for all their time, assistance, and support. Furthermore, I would like to thank my committee member, Dr. Karen Prestegaard, for her excellent advice and support. I would like to thank all the providers of data including United States Geological Survey (USGS), National Oceanic and Atmospheric Administration Chesapeake Bay Interpretive Buoy System (NOAA CBIBS), National Oceanic and Atmospheric Administration National Ocean Service (NOAA NOS), National Oceanic and Atmospheric Administration Center for Operational Oceanographic Products and Services (NOAA CO-OPS), Virginia Institute of Marine Sciences (VIMS), and University of Maryland Center for Environmental Science Horn Point Laboratory (UMCES-HPL).

Table of Contents

List of Tables

List of Figures

INTRODUCTION

Suspended sediments play an important role in maintaining estuarine ecosystems; for example, they provide nutrients to support productivity (Kemp et al., 2005) and facilitate marsh development through deposition (Donatelli et al., 2018; Redfield, 1972). However, excess suspended sediments can degrade water quality, limiting light availability to benthic organisms like submersed aquatic vegetation (SAV) (Cheng et al., 2013; Davis, 1985)**,** prevalent in many estuaries and coastal embayments. SAV provides nursing grounds for juvenile fish and a filter for suspended particles (Orth et al., 2010), enhancing water quality. Specifically, SAV reduces water current velocities and facilitates settling of smaller suspended particles (Sand-jensen, 1998), creating a positive feedback loop that enhances their resilience to storm events (Gurbisz and Kemp, 2014). Understanding feedbacks between sediment transport and SAV is integral to determining the ability of SAV to modulate water quality (Hirsch, 2012), especially by trapping terrestrial material otherwise bound for estuarine environments (Kemp et al., 2005).

In the upper Chesapeake Bay (CB), excess fine sediment is one of the main contributors to the degradation of water quality and adversely impacts habitats of living resources (Langland and Cronin, 2003). Anthropogenic activities have greatly influenced the supply of watershed sediments to the Susquehanna River (SR), the main tributary of CB, and subsequent delivery to upper CB (e.g. milldams, Conowingo Dam; Walter and Merritts, 2008; Zhang et al., 2016). However, the fate of sediment largely depends on biophysical processes within the SAV beds of the Susquehanna Flats (SF), which is the subaqueous delta of the SR at the head of CB.

Extensive SAV beds historically occupied SF but effectively disappeared following Hurricane Agnes in 1972. However, they have made a dramatic resurgence in the early 2000s (Gurbisz and Kemp, 2014), motivating several studies to determine their impact on sediment transport in the region (Bayley et al., 1978; Dennison et al., 2012; Gurbisz et al., 2016; Palinkas et al., 2014; Russ and Palinkas, 2018). These studies show that SAV does modulate suspended-sediment transfer from fluvial to estuarine environments by facilitating seasonal storage of material (Bayley et al., 1978; Gurbisz et al., 2016; Kemp et al., 2005; Russ and Palinkas, 2018), but the specific physical mechanisms active during storm events lack robust evaluation.

From mid-summer 2011 through late-fall 2011, a series of events provided the opportunity to examine these mechanisms. In particular, a significant wind event, Hurricane Irene (27-30 August 2011), provides insight into the impacts of wind events during times of low river flow. Then, from 7-16 September 2011, Tropical Storm Lee (TS Lee) produced significant precipitation over the SR watershed, leading to massive water (20,000 m^3 s^{-1}) and sediment discharges over the SF (Gurbisz et al., 2016) but relatively low winds. Approximately one month after TS Lee, a significant wind event enhanced water turbidity over the SF, likely via resuspension of fine particles deposited during TS Lee (Gurbisz et al., 2016; Russ and Palinkas, 2018).

In this study, we use the Coupled Ocean Atmosphere Wave Sediment Transport (COAWST) modeling system (Warner et al., 2010) with a flow-vegetation module (Beudin et al., 2017) to evaluate the impact of SAV on the transport of suspended sediment in the region. A necessary first step in using this relatively novel mechanistic model is to determine whether it can reproduce this dynamic environment at a high

resolution. Then, we investigate 4 scenarios to assess responses to different types of events with and without vegetation, as well as the impact of event timing: 1) a typical flow and wind pattern before Hurricane Irene, 2) a high-wind event associated with Hurricane Irene, 3) a high-flow event associated with the remnants of TS Lee, and 4) a high-wind event after TS Lee. Our overarching hypotheses are that sediment dynamics during typical and event conditions are significantly different and that the sequence of events is crucial to those impacts. Additionally, the existence of plants over the region modulate flow and sediment transport to the rest of CB by reducing current speeds, therefore enhancing sediment deposition, and acting as a temporary holding area for fine particles (Gurbisz et al., 2016).

Calibrating and evaluating the COAWST system provides an open-source approach to investigating the complex interactions within this highly dynamic fluvial-estuarine interface. By evaluating the various mechanisms controlling sediment retention and erosion within the region during storm events, potential impacts to downstream ecosystems can be better predicted to aid in management efforts.

METHODS

Site description

The Susquehanna Flats region is the subaqueous delta of the Susquehanna River (SR) located at the tidal headwaters of the Chesapeake Bay (CB) (Figure 1). The depositional basin of the Flats has a bowl-shape geometry covering roughly 89 km^2 (Davis, 1985) with a primary channel along the western side approximately 3-7 meters deep (Gurbisz and Kemp, 2014). Physical processes in this region are influenced primarily by the flow of the SR, which has an average discharge of 1,100 $m^3\ s^{-1}$

(Schubel and Pritchard, 1986) and is the largest source of sediment to the upper CB (Figure 1). The SR typically has its highest discharge in spring from snow melt and spring rains followed by low-to-moderate flow for most of the year (Gross et al., 1978). Tidal currents with mean tidal range of 0.6 m (Bayley et al., 1978), wave action with significant wave heights < 1 m and a mean period of < 2.5 s (https://buoybay.noaa.gov/), and seasonal vegetation (Bayley et al., 1978; Gurbisz and Kemp, 2014) also play significant roles in sediment transport in upper CB. In particular, vegetation reduces currents and wave activity, facilitating sediment deposition (Gambi et al., 1990; Granata et al., 2001; Peterson et al., 2004). Historically, the Flats had a large distribution of vegetation; however, this population was decimated by Hurricane Agnes in 1978. There was a resurgence of SAV in the mid-2000s (Gurbisz and Kemp, 2014). Recent work has highlighted the ability of SAV to trap sediments, modulating sediment input into CB (Russ and Palinkas, 2018).

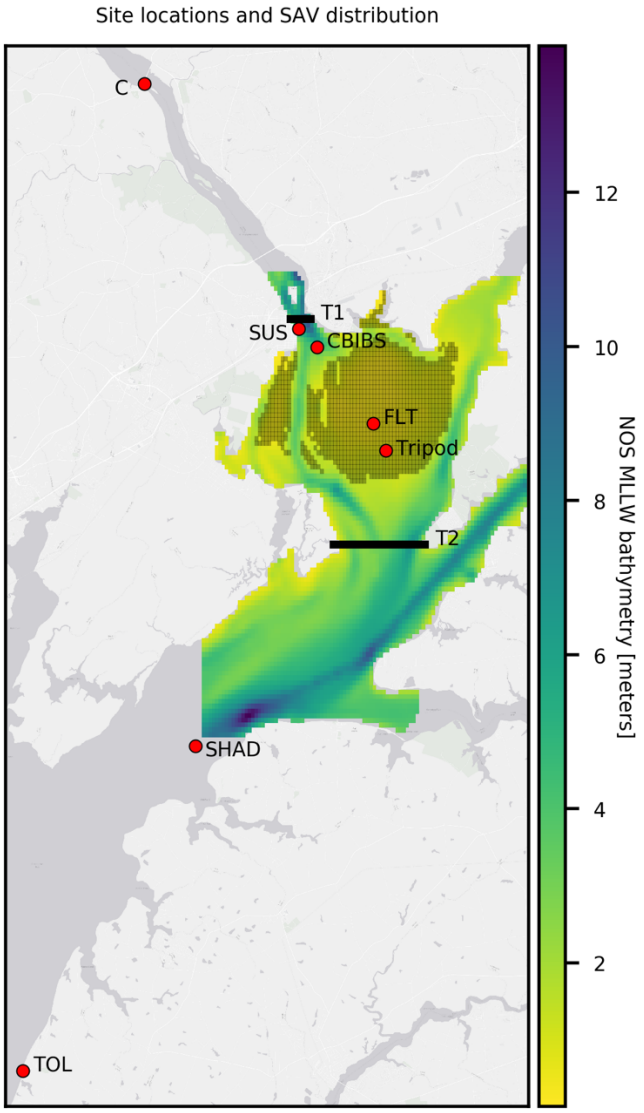

Figure 1: Map of study region with points denoting the locations of USGS Conowingo Dam discharge observations (C), turbidity observations from Maryland Department of Natural Resources Chesapeake Bay-Segment 1 Susquehanna Flats (FLT) and Susquehanna River – Havre de Grace (SUS), wind and current observations (CBIBS), wave observations from 2013 (Tripod), surface elevation prediction (SHAD), and surface elevation measurement (TOL). Lines T1 and T2 are the transects used in the flux calculations at the entrance and exit of the system, respectively. The colors indicate the NOAA NOS MLLW bathymetry, in meters, scaling from shallow water (yellow) to deep water (green), used for model initialization. The vegetation patch supplied to the model is the grey shaded region.

The SR has 50-75% of the annual sediment load contributed to the CB. The total load is composed of 10% sand, 50% silt, and 40% clay, transported during peak stream discharge, with fine material clearly dominating the sediment loading (Chesapeake Research Consortium, 1976; Williams and Reed, 1972). On the Flats, surficial sediments

are sandy, with median diameters ranging from 113.1 μm to 405.3 μm and generally decreasing with distance from the river mouth (Russ and Palinkas, 2018; Sanford et al., 2007). However, fine sediment was observed in the middle of the vegetation in regions of high sedimentation rates, ~1 g cm^{-2} y^{-1} (Russ and Palinkas, 2018).

The variety of wind and river discharge magnitudes from late summer and through the fall of 2011 provide insight into potential controlling mechanisms for sediment transport and deposition (Table 1 and Figure 2). From mid-July to late-August, wind velocities and river discharges were both relatively low ("before Irene"), representing typical summer conditions. Then, Hurricane Irene passed through the region at the end of August, with sustained maximum winds of 14 m s^{-1} but low river discharge ("Irene"). This was followed by the passage of the remnants of Tropical Storm (TS) Lee in early September ("Lee"), which brought much rainfall but little wind to the region. SR discharge peaked at 20,000 m^3 s^{-1} during this event, the second highest discharge on record. Finally, a wind event occurred in mid- to late-October that had sustained winds of 10.5 m s^{-1} and moderate river discharge ("Post-Lee"). In this study, we take advantage of the different environmental conditions associated with each event to investigate potential controlling mechanisms on sediment transport and deposition.

Table 1: Description of the wind and river discharge conditions during each event encompassing the time period from start date to end date. High indicates the dominant forcing during the event.

Event	**Wind**	**Discharge**	**Start date**	**End date**
Before Irene	Low	Low	2011-08-01	2011-08-06
Irene	High	Low	2011-08-27	2011-08-30
Lee	Low	High	2011-09-07	2011-09-16
Post-Lee	High	Moderate	2011-10-13	2011-10-24

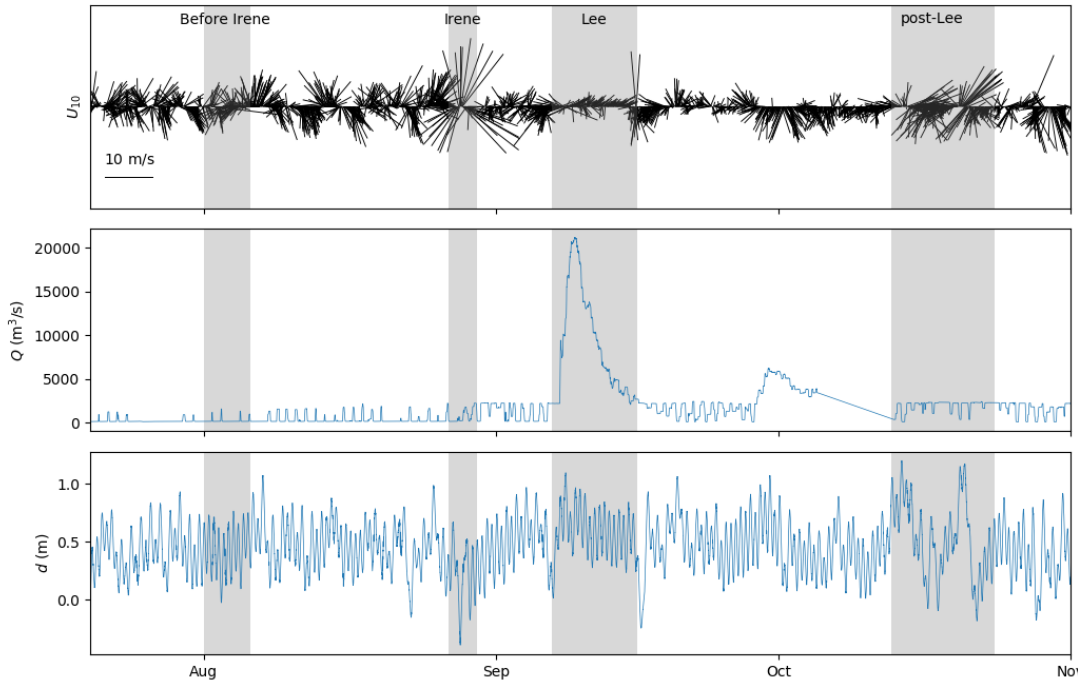

Figure 2: Stacked plot of the model forcing used throughout the simulation with the events from Table 1 highlighted in grey. The top panel represents a stick vector plot of the wind velocities at the NOAA-NOS CBIBS Susquehanna station (U_{10}). The middle panel represents the river discharge observations from the USGS sensor at Conowingo Dam (Q). The bottom panel represents the phase adjusted Tolchester Beach water surface elevation observations (d).

COAWST description and initialization

This study uses the Coupled-Ocean-Atmosphere-Wave-Sediment Transport (COAWST) modeling system (Warner et al., 2010) to evaluate the impacts of vegetation on sediment transport and deposition during the 2011 events on the Flats. The COAWST modeling system is composed of several community developed model components, including the Regional Ocean Modeling System (ROMS; Shchepetkin and McWilliams, 2005), Simulating Waves Nearshore (SWAN; Booij et al., 1999), Weather Research and Forecasting Model (WRF; Skamarock et al., 2005), and the Community Sediment Transport Modeling System (CSTMS; Warner et al., 2008). For this study, the ROMS-SWAN-CSTMS components were used to investigate interactions among currents, waves, sediment and vegetation. New vegetative components were recently implemented

in the ROMS, namely plant posture-dependent three-dimensional drag, vertical mixing, and wave-induced streaming (Beudin et al., 2017).

As detailed in Chen et al. (2007), various models have been developed to simulate flow through vegetation, but each has its limitations. The implementation by Beudin et al. (2017) attempts to resolve these limitations through a coupled approach. This is accomplished by sending the wave-energy dissipation due to vegetation, calculated in SWAN, into the ROMS momentum balance as an additional wave-averaged forcing (Beudin et al., 2017). This formulation allows for the flow through vegetation to be calculated based on the flexibility of the vegetation, instead of an enhanced bottom roughness used previously (Morin et al., 2000). The impacts of flexible vegetation account for the observed wave-energy dissipation from the drag force on the vegetation, which modifies the wave characteristics (Beudin et al., 2017).

COAWST was initialized similar to the scenario described in Beudin et al. (2017) across 18 parallel nodes. The model grid, used in both ROMS and SWAN, was established as a rectangular grid, with a longitudinal distance of 16.49 km and a latitudinal distance of 23.76 km, evenly divided into 100x100 cells and 5 layers in topography following sigma-coordinates (Figure 3). The simulation was executed from 19 July, 2011 through 1 November, 2011 with time steps of 30 seconds for both ROMS and SWAN with coupling every 30 seconds. The precise start date and time was selected due to the zero meter peak low tide relative to mean lower low water, which is the reference for the bathymetric grid; and the end date was selected to encompass the "post-Lee" wind event.

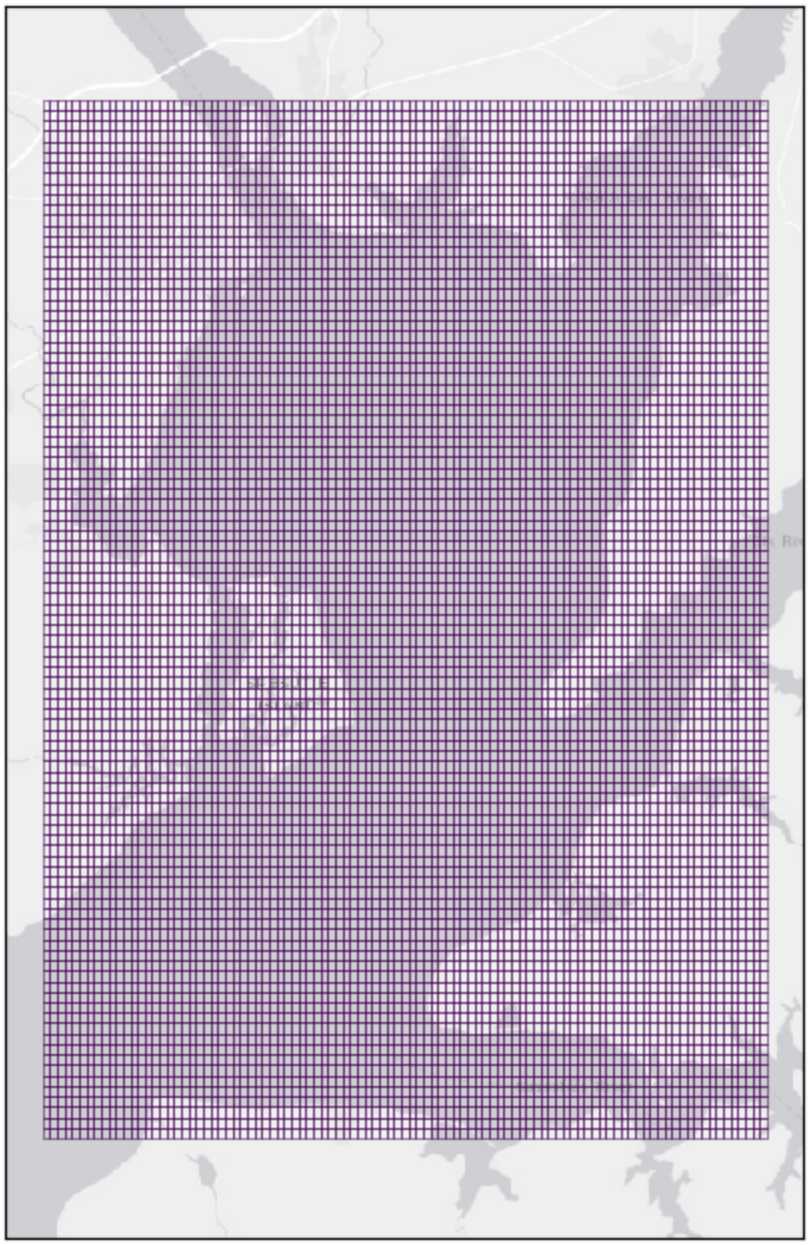

Figure 3: Geospatial map of the model grid.

Bathymetry was obtained from the National Oceanic and Atmospheric Administration's National Ocean Service, 30-meter resolution Digital Elevation Model (https://ngdc.noaa.gov/mgg/bathymetry/estuarine/index.html) (National Centers for Environmental Information, 2017) (Figure 1). Using GridBuilder v0.99, the land cells were established as masks using the Global Self-consistent Hierarchical High-resolution

Geography (GSHHG) coastline in combination with manual manipulation of grid cells for accurate depiction of the coastline (Wessel and Smith, 1996).

Submersed aquatic vegetation (SAV) distributions over the study area were obtained from the 2010 annual SAV survey by the Virginia Institute of Marine Sciences (VIMS). Data were downloaded from the VIMS Chesapeake Bay Submersed Aquatic Vegetation distribution site (http://web.vims.edu/bio/sav/gis_data.html). Areas with 70-100% SAV coverage and water depths less than 2 meters (Kemp et al., 2004; Kreiling et al., 2007) were included as vegetated cells in the model (Figure 1). Vegetation characteristics were assigned from field observations of the dominant species *Valisneria americana* (Catling et al., 1994; Gurbisz et al., 2016; Gurbisz and Kemp, 2014). Specifically, average vegetation height, diameter, thickness, and density were 0.305 m, 0.001 m, 0.001 m, and 100 stems m^{-2}, respectively (Lovett-Doust and Laporte, 1991). With the implementation of flow through vegetation as established by Beudin et al. (2017), a singular vegetation type with stem flexibility (elastic modulus) of 1.0 GPa was used, as estimated in Luhar et al. (2008) for similar submersed vegetation. The drag coefficients for ROMS and SWAN were set to 1.0, which is the typical value for a cylinder at high Reynolds number, which occurs for typical current velocities in the region. Mass density was established as 700 kg m^{-3} (Beudin et al., 2017), and the additional horizontal viscosity coefficient at the edge of the vegetation patch was set to 0.10 (Beudin et al., 2017).

ROMS sediment characteristics were established using two sediment classes, cohesive mud (referred to as "fine sediment"; D50 = 4 μm) and noncohesive sand (referred to as "coarse sediment"; D50 = 375 μm) with specific properties established

with average values from field observations (Table 2; Palinkas et al., 2014). The simulation neglected the effects of flocculation due to the limited flocculation of particles in this high energy system. Additionally, bedload transport was not turned on since the focus of this effort was to evaluate suspended sediments. Due to complex near-bed wave-orbital characteristics during the simulation period, the bottom boundary layer was established using the wave-current bottom boundary layer model (Beudin et al., 2017; Madsen, 1995).

Table 2: Initialization parameters for the fine (Clay-cohesive) and coarse (Sand-noncohesive) sediment for ROMS. The parameters indicated with an asterisk (*) are from Palinkas et al. (2014).

	fine	**coarse**
D50 (μm)	4	375
Grain Density (kg/m^3)	2650	2650
Settling Velocity (mm/s)*	0.02	0.85
Erosion Rate (kg/m^2/s)*	4x10^{-5}	4x10^{-5}
Critical stress erosion (N/m^2)*	0.049	0.09
Critical stress deposition (N/m^2)*	0.049	0.09
Porosity	0.9	0.5
SSC (kg/m^3)	(*Eqn. 1*)	(*Eqn. 2*)

The initial sediment bed was established with three existing sediment layers: a 1-cm thick active-mixed layer composed of 13.24% fine and 86.76% coarse, overlying a 1-cm thick coarse layer to act as a transition to a 99-cm thick coarse layer, as observed by Russ and Palinkas (2018). During model initialization, no other suspended sediment was supplied throughout the grid space. Therefore, all suspended sediment during the simulation was from either SR suspended sediment or resuspended sediment from the existing bed layers. Suspended-sediment concentration (SSC) data for the SR were not available for the entirety of the model simulation. Instead, the empirical relationship between SSC and SR discharge during high-flow by Cheng et al. (2013) was

implemented; SSC was separated into the two size classes following Palinkas et al. (in press) and using Eqs. 1 and 2 below.

$$f_{fine} = SSC \times (-0.941 \times 10^{-5} Q + 0.983) \quad (1)$$

$$f_{coarse} = SSC \times (0.941 \times 10^{-5} Q + 0.017) \quad (2)$$

The ROMS boundary conditions for the northern and western edges were established as gradient conditions for the free-surface and depth-averaged velocities, which sets no variation at the boundary and simplifies computational complexity. The southern boundary was established as a Chapman Explicit condition for the free-surface, which allows the free surface to vary based on input data (Hedström, 2009), and Flather for the depth-averaged velocities as recommended for river outflow (Hedström, 2009). The velocity, temperature, salinity, and sediment were established as gradient conditions across all boundaries. Since the main interest of this study is the flow of SR water and sediment, the North East River and Elk River were masked to reduce possible sources of error.

The tide forcing was established as a boundary condition along the southern grid using the water-elevation data from the NOAA CO-OPS station Tolchester Beach (station id: 8573364 https://tidesandcurrents.noaa.gov/stationhome.html?id=8573364) phase-shifted to the model grid. The phase shift was accomplished by using the NOAA Chesapeake Bay Operational Forecast System (CBOFS) forecasted water elevations for Tolchester Beach and Shad Battery (a point near the model boundary) (Figure 1 and Figure 4). After comparing various temporal adjustments, a positive shift of 78 minutes to the Tolchester Beach forecast elevation data resulted in a matching of the high and low

tides to the Shad Battery forecasted elevations (Figure 4). The amplitude of the surface elevation was adjusted according to (3).

$$z_2 = c\left(z_1 - z_{1\,avg}\right) + z_{1\,avg} \tag{3}$$

where, z_1 is the elevation at the initial point (Tolchester Beach), $z_{1\,avg}$ is the average elevation at the initial point during the time series, *c* is the adjustment factor, and z_2 is the elevation at the point of interest. For this study a value of 1.1 (a 10% increase) for the adjustment factor *c* lead to agreement between the adjusted Tolchester Beach predictions (z_1) and the model boundary Shad Battery predictions (z_2) (Figure 4; Lee et al., 2017). Tides were forced relative to mean lower low water, the reference for the bathymetry data, varying the surface strictly above mean lower low water (Figure 4). The historical data from CBOFS dates back to 2014, therefore the September 2014 predictions were used to establish this relationship since seasonality and river discharge has a large impact on water level variations in the region on decadal scales (Barbosa and Silva, 2009).

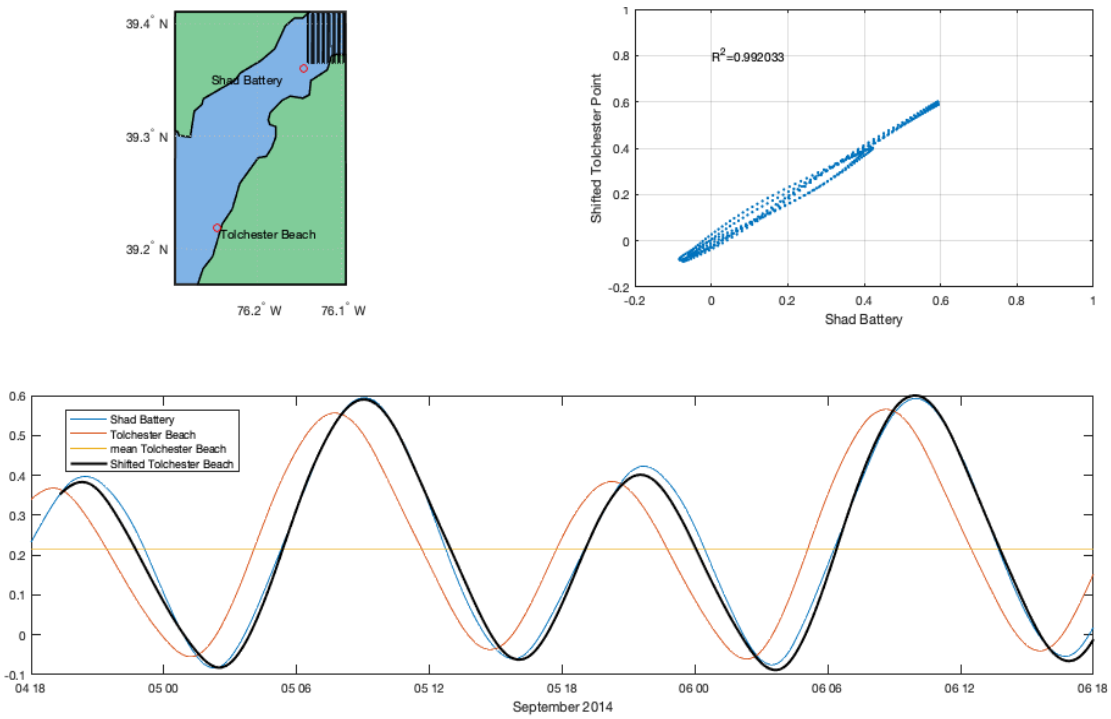

Figure 4: Time series of surface water elevations, 4 September through 6 September 2014, from the Chesapeake Bay Observational Forecast System (CBOFS) tidal predictions (bottom) with Tolchester Beach predictions (red), Shad battery predictions (blue) and the translated Tolchester Beach predictions to match the Shad Battery predictions using Eqn (3) (black). The upper right panel is a comparison between the shifted Tolchester Beach elevations (y-axis) and the Shad Battery elevations (x-axis) with $R^2 = 0.992$. The upper left panel is a map of the Tolchester Beach and the Shad Battery prediction locations (red circles) within CB and the edge of the model grid (black vertical striations).

SWAN was established in nonstationary mode using GEN3 physics, vegetation, and forced by wind input from observations, as described below. For this study, only the wind observations from *in-situ* stations were used to perturb the system. Due to the region being fetch limited (Sanford, 1994) and its typical wave characteristics, the Komen method for wave dissipation (Komen et al., 1984), with a frequency range from 0.2 to 2 Hz with 24 meshes in frequency space, was established to capture small wave periods and small wave heights, which is vital for this region (Fisher et al., 2015).

For river discharge, *in-situ* observations from the USGS gauge at the Conowingo Dam outlet (https://waterdata.usgs.gov/usa/nwis/uv?01578310) were adjusted according to (4):

$$Q = (Q_{obs}/n_{rivers}) * 0.8 \quad (4)$$

where, Q_{obs} is the observed river discharge from the Conowingo station in $m^3\ s^{-1}$, n_{rivers} is the number of river grid cells over which the flow is distributed (Harris et al., 2008; Liu and Wang, 2014; Xue et al., 2012), and 0.8 represents a 20% reduction in flow. This was forced into ROMS as a horizontal momentum transport point source. The 20% reduction was needed to align the simulated current velocities with observed values at CBIBS Susquehanna Station (Figure 5), as determined during development of the discharge model, similar to the adjustments made for the Hudson River simulations from Warner et al. (2005). The timing of the river discharge was phase shifted by 2 hours to account for the 11.3 km distance downriver from the Conowingo Dam to the model's northern boundary (Figure 1 and Figure 5).

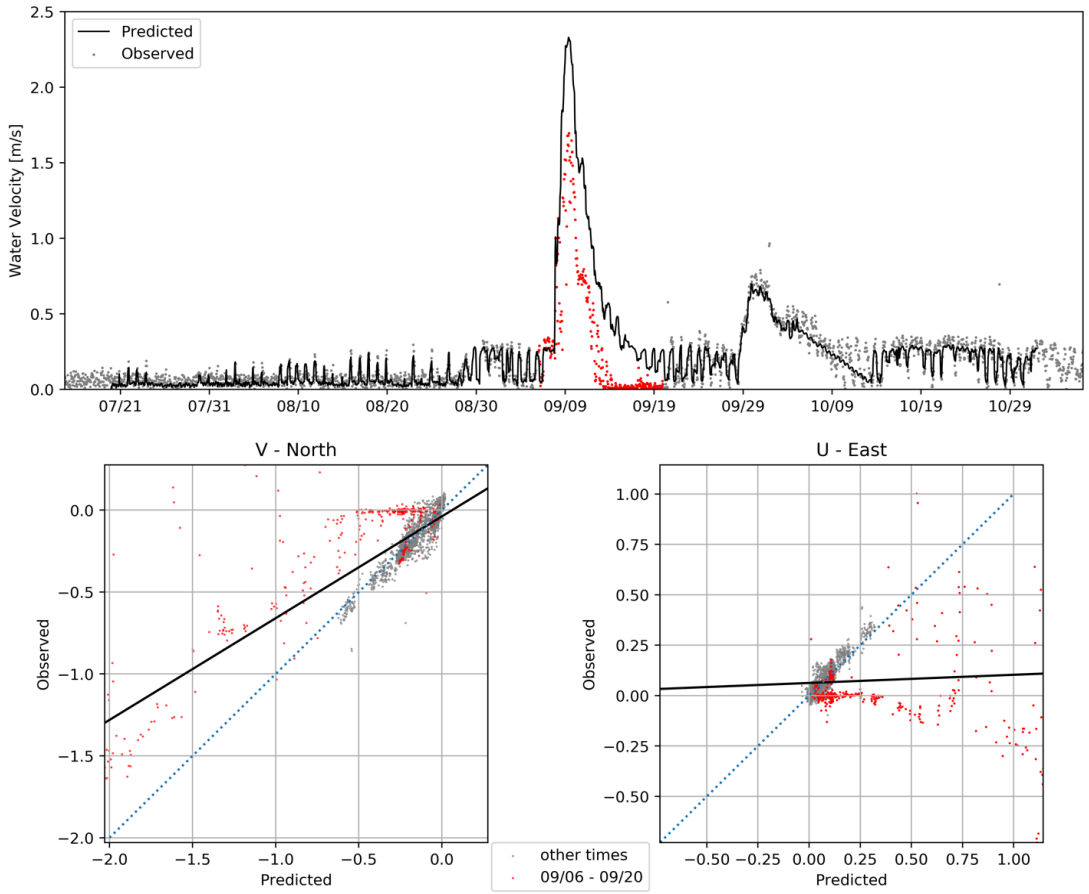

Figure 5: Timeseries (top panel) of the magnitude of the water velocity (m/s) from CBIBS bin 2 ADCP observations (dots) and the respective location within the model grid (black line). The bottom two panels are comparisons between the observations (y-axis) and the model predictions (x-axis) (m/s), for the North (left panel) and East (right panel) components of the water velocity (m/s). The red dots indicate the velocities between 6 September and 20 September and the black dots are the observations outside that time interval. The black line is the linear regression of the observed and predicted velocity components for the entire simulation (black and red dots combined) and the dashed blue line is the 1:1 line.

Wind forcing for the SWAN portion of the simulation was established from the CBIBS Susquehanna station wind observations, which were adjusted from an observation height of 3 m to an observation height of 10 m, as required by SWAN, using the power-law profile (Figure 2) (Hsu et al., 1994; Kilbourne, 2017). The 10-meter velocities were applied to the model grid as spatially-invariant constant wind speeds every 10 minutes.

The model was configured to simulate the conditions from August to November 2011 listed in Table 1. The conditions include typical wind and river discharges, a significant wind event (end-August, Hurricane Irene) followed by a large river-discharge

event (early-September, Tropical Storm Lee), and another significant wind event with moderate river discharge (mid-October) (Figure 2). Two scenarios were run for each condition: one with vegetation ("veg"), and one without vegetation ("no-veg"). Both of these used all of the sediment, river discharge, and wind conditions. However, only the vegetated scenario used the vegetation patch and vegetation module during model initialization.

Model performance was evaluated at site CBIBS and Tripod (see RESULTS); the impact of vegetation was assessed at site FLT on the Flats (Figure 1). Additionally, sediment characteristics were evaluated by calculating imports/exports and geospatial differences by sub-setting the model domain to a region between two transects: the mouth of the Susquehanna River (T1 in Figure 1), and a longitudinal transect between Turkey Point and Sandy Point (T2 in Figure 1). These two transects, represent the entrance and exit from the Flats system, respectively. For each event, the bed elevation and mass change were calculated as the difference between the final and initial values at each cell during the selected time period. The sediment budget was determined by computing the cumulative southward flux of sediment, by class, and integrating over the specified time interval resulting in total metric tons crossing southward at the transect.

RESULTS

Model validation

To validate model-predicted currents, depth-averaged velocities from the full model simulation and in-situ velocity observations from the Chesapeake Bay Interpretive Buoy System (CBIBS) at station Susquehanna were compared (Figure 5). Highest velocities in both time series occurred during TS Lee in September 2011, due to

widespread, enhanced precipitation over the SR drainage basin. However, the CBIBS observations during the event were flagged as questionable. Along-channel velocity increased with river flow during the event, but across-channel flow indicated an increase perpendicular to the river channel. Additionally, the distribution of velocity observations over the east and north axis of flow do not follow along the axis of flow (from the northwest to the south east) as expected. Therefore, CBIBS observations during this event are not representative of known river current velocities. However, the north and east velocities from the model before 6 September and after 20 September (Figure 5) align well with the north and east velocities from the CBIBS platform (Figure 5). Indeed, these observations and model predictions fall along the 1:1 line in Figure 5, while observations between 6 and 20 September are much lower than predictions.

To validate the performance of the wave model (SWAN), an additional simulation was performed for July 2013, when direct observations of the wave environment were available (Sanford, unpub. data). The wave model was configured as described in the methods with the following adjustments to account for the specific characteristics of the region in 2013. Since tidal forcing was not included in this simulation, the water depth was uniformly increased by 0.4 meters to adjust the reference water level from mean lower low water to mean tide level to resolve limited wave propagation in shallow water. Additionally, vegetation was not included in the wave configuration since it was absent during the 2013 observational period (http://web.vims.edu/bio/sav/sav13/quads/ss009th.html). The 2013 wave-model predictions agree well with the in-situ observations (Figure 6). Specifically, agreement in the rapid increase and decrease in significant wave heights and peak wave periods

associated with a change in wind direction and speed indicated the model's responsiveness and accuracy in this dynamic wind environment.

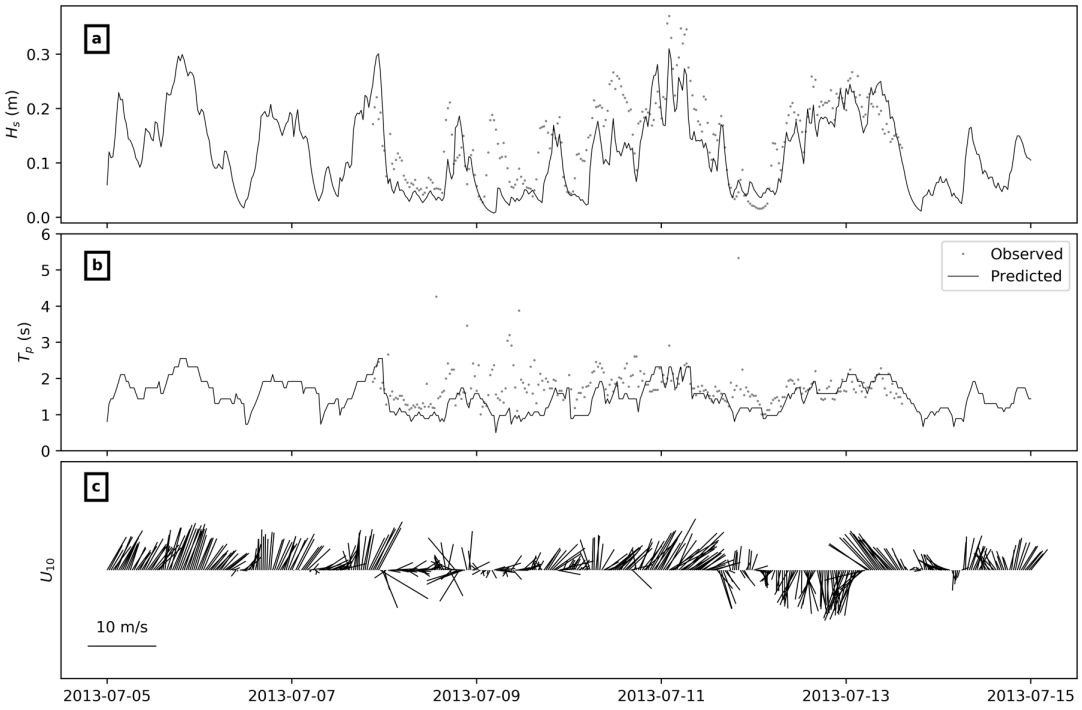

Figure 6: Comparison of (a) significant wave height (H_s) and (b) peak wave period (T_p) for (c) observed winds (U_{10}) from the tripod platform (grey dots) and SWAN model predictions for the same location (black line)

Event Dynamics

To evaluate the dynamics of each event, the model results were inspected by 1. time series analysis at the Maryland Department of Natural Resources Susquehanna Flats site (FLT); 2. geospatial changes of the sediment bed layer, depth averaged water velocity, fine and coarse SSC, and significant wave heights; and 3. evaluation of sediment fluxes entering and exiting the system. By inspecting the model using these three classifications, we provide validation that the model recreated the physical environment and determined that is can be used to evaluate the impact of vegetation and timing during the four events.

Typical Conditions

Under typical conditions ("before Irene" in Table 1), wave and current magnitudes were low, indicating low energy conditions (Figure 7). Vegetation on the Flats generated a nearly 30% reduction of current speeds within the patch, which results in the bottom stresses being cut nearly in half (Figure 7). Maximum wave and current induced bottom stress magnitude showed stresses exceed the critical value for erosion of fine sediment of 0.049 N m^{-2} under non-vegetative conditions, resulting in increased suspended sediments in both classes (Figure 7). Fine sediment concentrations reached 0.05 kg m^{-3} under non-vegetative conditions as compared to nearly 0 kg m^{-3} with vegetation. At peak current velocities (during ebb tide and a discharge event on 2011-08-02 21:00), current speeds reached a maximum of 0.49 m s^{-1} under vegetative conditions and 0.42 m s^{-1} under non-vegetative conditions in the main channel primarily due to the vegetation focusing the flow into the channel (Figure 8). Vegetation did modulate the current velocities, which resulted in less fine material in suspension over the vegetated region at peak current velocities (Figure 9). There was net export of sediment from the system, primarily in the fine-sediment class (Table 3), which was enhanced under non-vegetative conditions, but also in the coarse-sediment class. Interestingly, under vegetative conditions, coarse material was retained within the system (Table 3). The change in the fine-sediment bed-layer mass showed removal in the main channel under vegetative conditions, and slight removal over the shallow flats under non-vegetative conditions indicating local resuspension (Figure 10).

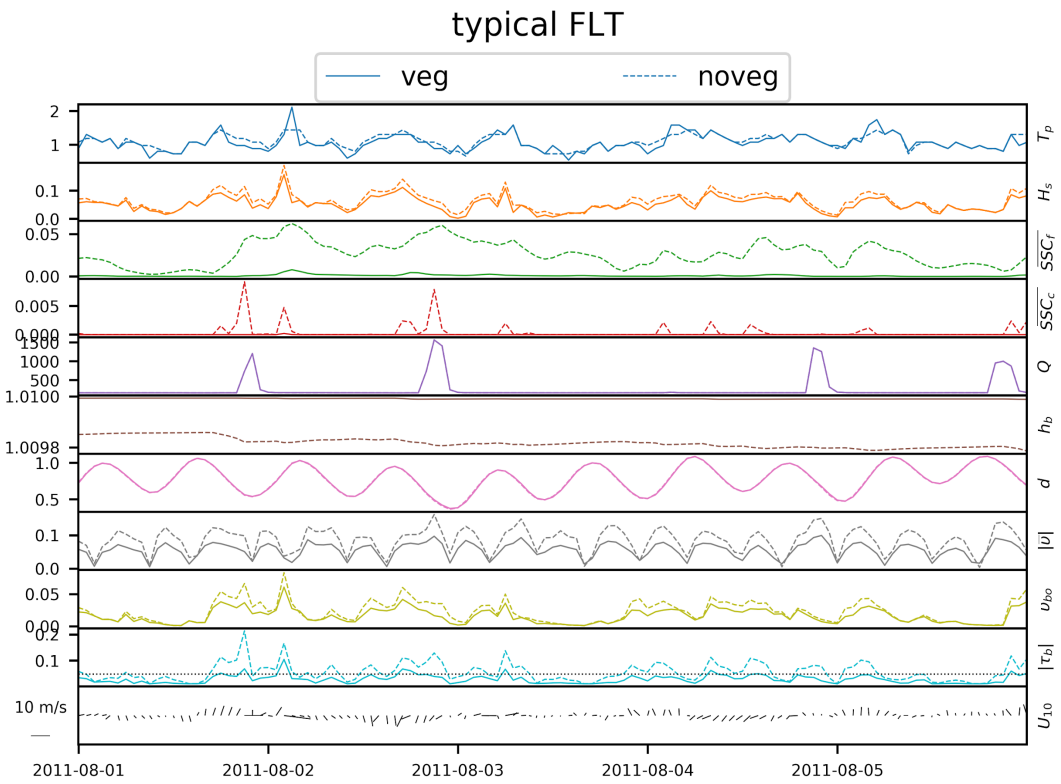

Figure 7: Model prediction summary for FLT during typical conditions with vegetation (solid) and without vegetation (dashed). From top to bottom the parameters are; T_p - Peak wave period (s), H_s - Significant wave height (m), SSC_f - Depth averaged fine sediment concentration (kg/m^3), SSC_c - Depth averaged coarse sediment concentration (kg/m^3), Q - River discharge (m^3/s), h_b - Bed thickness (m), d - Total water depth (m), $|\bar{v}|$ - Depth averaged current magnitude (m/s),v_{bo} - Wave-induced bottom orbital velocity (m/s), $|\tau_b|$ - Maximum wave and current bottom stress magnitude (N/m^2) with a dotted line indicating the critical shear stress of 0.049 N/m^2, and U_{10} - Wind speed and direction (m/s).

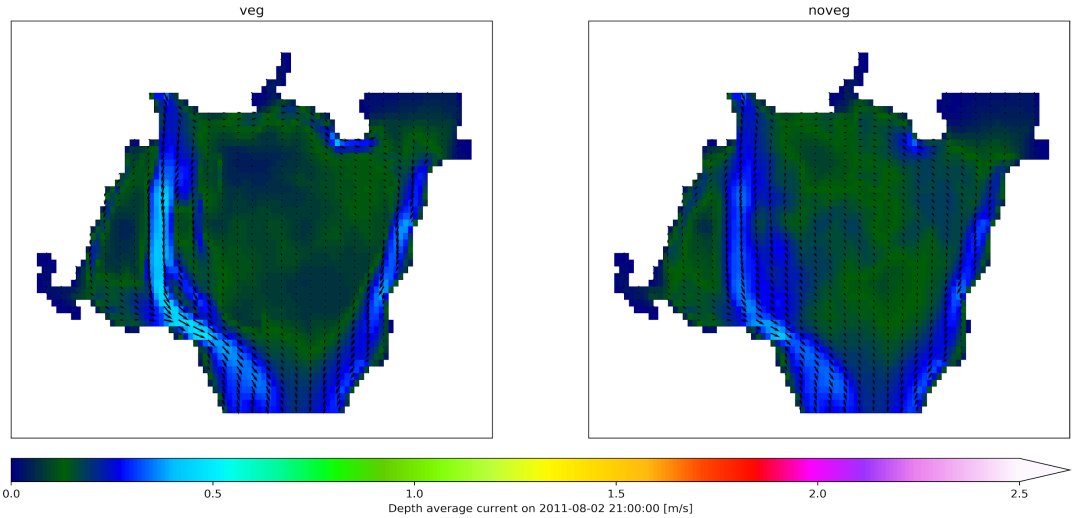

Figure 8: Spatial distribution of depth averaged current speeds (m/s), from low (green) to high (pink/white), with velocity vectors, to indicate direction, during a discharge event and peak ebb tide from before Irene, on 2 August 2011 at 21:00, under vegetative (left panel) and non-vegetative (right panel) conditions.

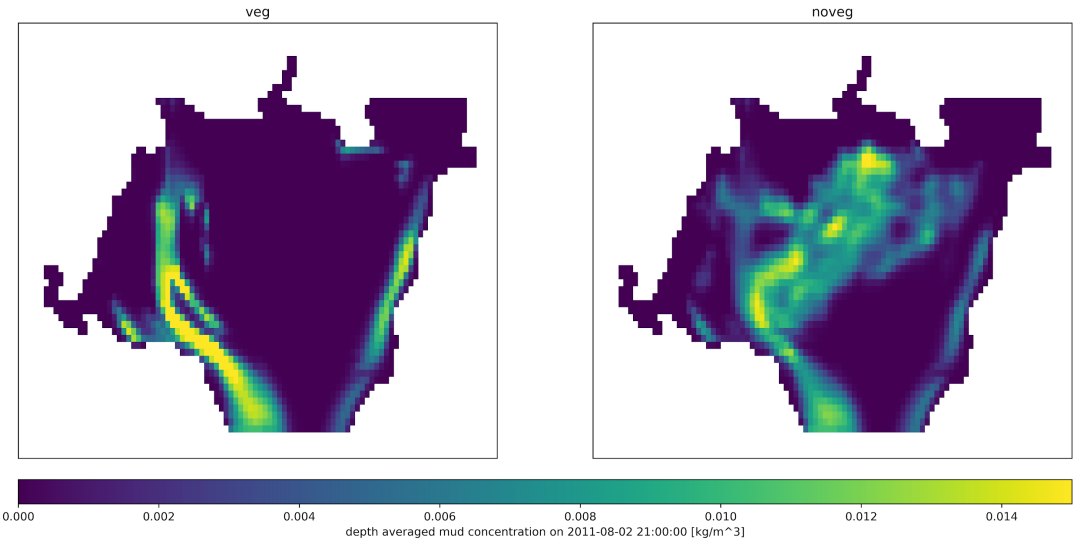

Figure 9: Spatial distribution of the depth averaged concentration of mud (kg/m^3), from low (blue) to high (yellow), during the discharge and ebb event on 2 August 2011 at 21:00 under vegetative (left) and non-vegetative conditions (right).

Table 3: Southward time integrated flux, in metric tons, for each sediment class during vegetative and non-vegetative conditions. T1 and T2 indicate which transect the flux is computed across and the event is the selected time period of calculation (see Table 1). T1-T2 is the difference, in metric tons, between T1 and T2 under the specified conditions.

		Vegetative		***Non-Vegetative***	
	event	**fine (T)**	**coarse (T)**	**fine (T)**	**coarse (T)**
T1	Before Irene	642	18	642	17
T2	Before Irene	1607	3	1773	37
T1-T2		**-665**	**15**	**-1131**	**-20**
T1	Irene	2769	901	2769	869
T2	Irene	10420	774	15828	833
T1-T2		**-7651**	**127**	**-13059**	**36**
T1	Lee	4255870	1828650	4256099	1886315
T2	Lee	4101554	870441	4168703	730231
T1-T2		**154316**	**958209**	**87396**	**1156084**
T1	Post-Lee	29552	18395	29551	17255
T2	Post-Lee	37503	5619	33104	4437
T1-T2		**-7951**	**12776**	**-3553**	**12818**

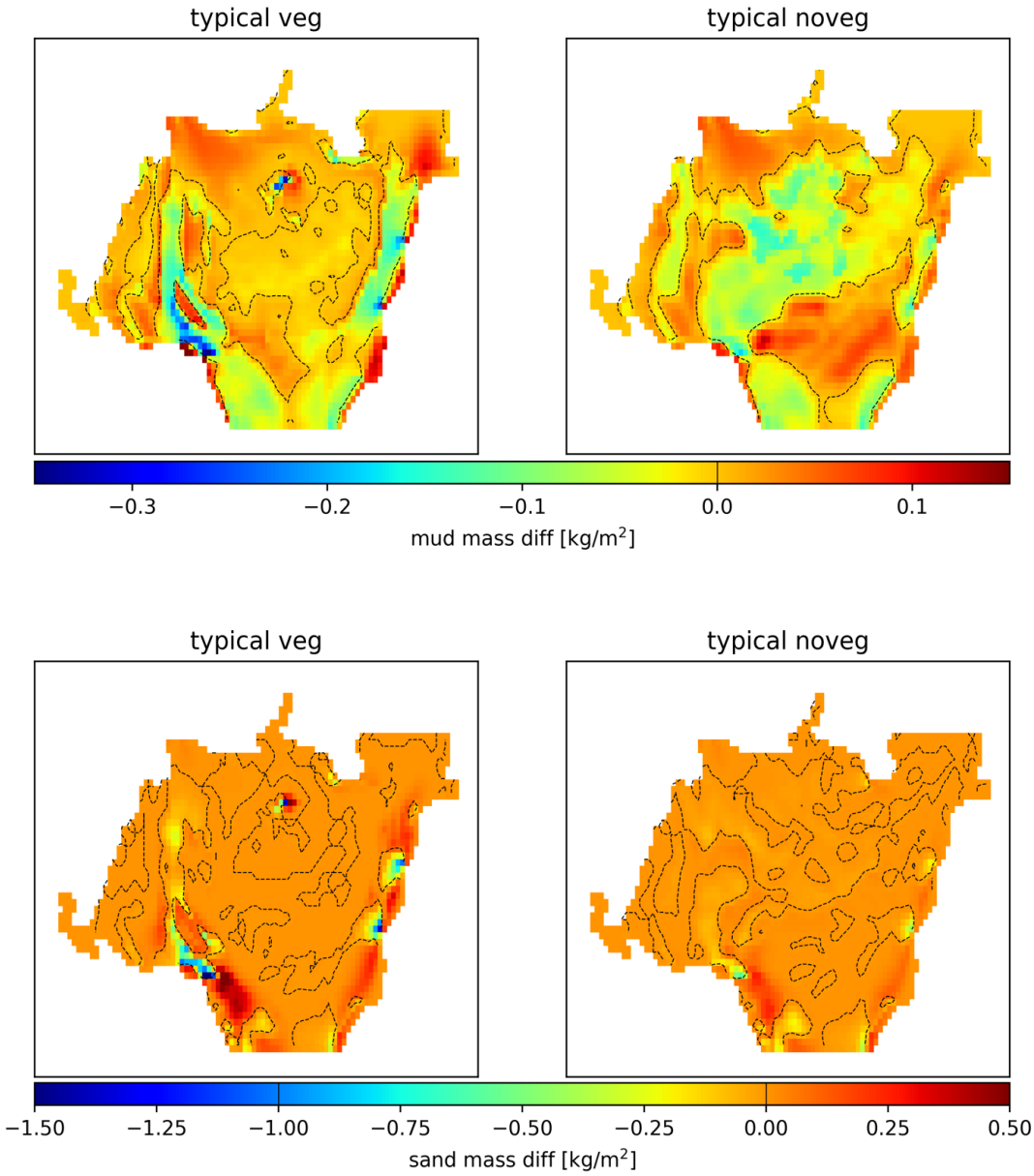

Figure 10: Spatial distribution of the mud mass difference (kg/m^2) between the final and initial mass in the bed layer sum over the time period associated with typical conditions, under vegetative (left) and non-vegetative (right) conditions. Coloring indicates removal of mass (blues and greens) and addition of mass (reds) over the time period. A dashed line is included in both panels to indicate the delineation between removal and addition of mass.

Hurricane Irene

During Hurricane Irene, river discharge was low (average 780 ± 722 m^3 s^{-1}) and winds were high, peaking at 14.4 m s^{-1} on 28 August at 13:00 (Figure 11). On 28 August at 08:00 the water depth at the FLT site approached zero meters, resulting in difficulties

in the modeling effort and some questionable responses for a short period of time. However, responses before and after the peak low tide event were representative of the system by quickly rebounding to appropriate current speeds and wave heights. Bottom stress was enhanced by an order of magnitude in the non-vegetated scenario (Figure 11 and 12), leading to an increase in suspended material (Figure 11). When vegetation was present the bed elevation increased within the vegetation patch, but showed signs of decreasing in the same region, when vegetation was not present (Figure 13). Differences in bed mass occurred mostly in the fine-sediment class, increasing with vegetation and decreasing in the absence of vegetation, with little differences in the coarse-sediment class (Figure 14). Additionally, there was net transport of fine sediments out of the region and retainment of coarse sediments within the region (Table 3). The vegetation enhanced the retainment of coarse material and reduced the export of fine material (Table 3). Significant wave heights during peak winds (Figure 15) exceeded heights of 0.5 m with clear delineation, via wave height reduction, of vegetation.

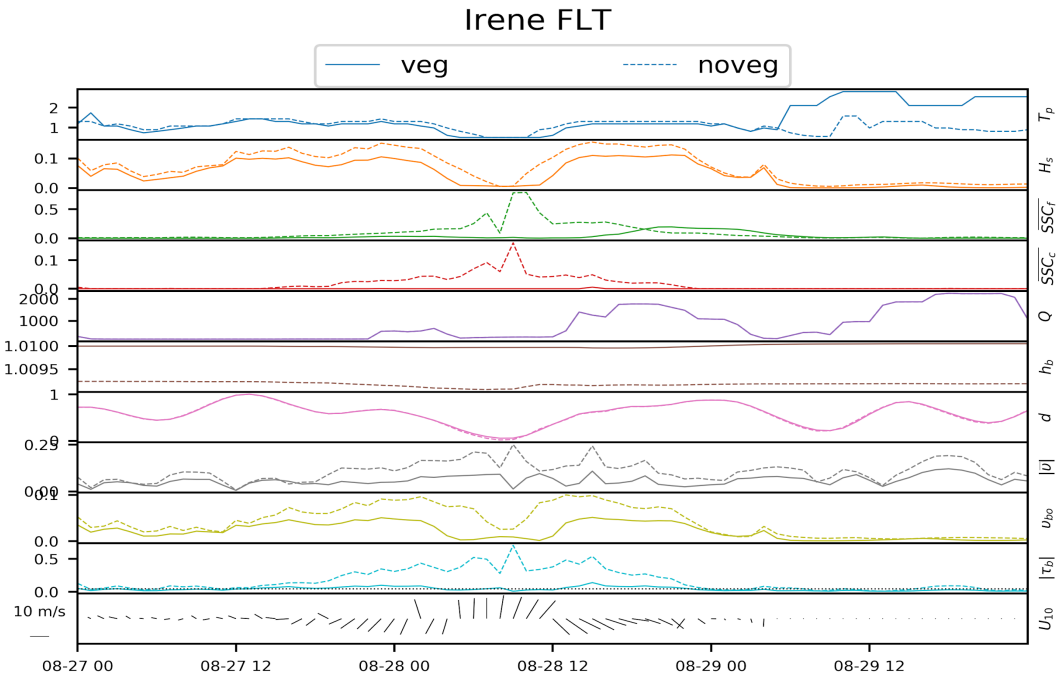

Figure 11: Model prediction summary for FLT during Irene with vegetation (solid) and without vegetation (dashed). From top to bottom the parameters are; T_p - Peak wave period (s), H_s - Significant wave height (m), SSC_f - Depth averaged fine sediment concentration (kg/m^3), SSC_c - Depth averaged coarse sediment concentration (kg/m^3), Q - River discharge (m^3/s), h_b - Bed thickness (m), d - Total water depth (m), $|\bar{v}|$ - Depth averaged current magnitude (m/s),v_{bo} - Wave-induced bottom orbital velocity (m/s), $|\tau_b|$ - Maximum wave and current bottom stress magnitude (N/m^2) with a dotted line indicating the critical shear stress of 0.049 N/m^2, and U_{10} - Wind speed and direction (m/s).

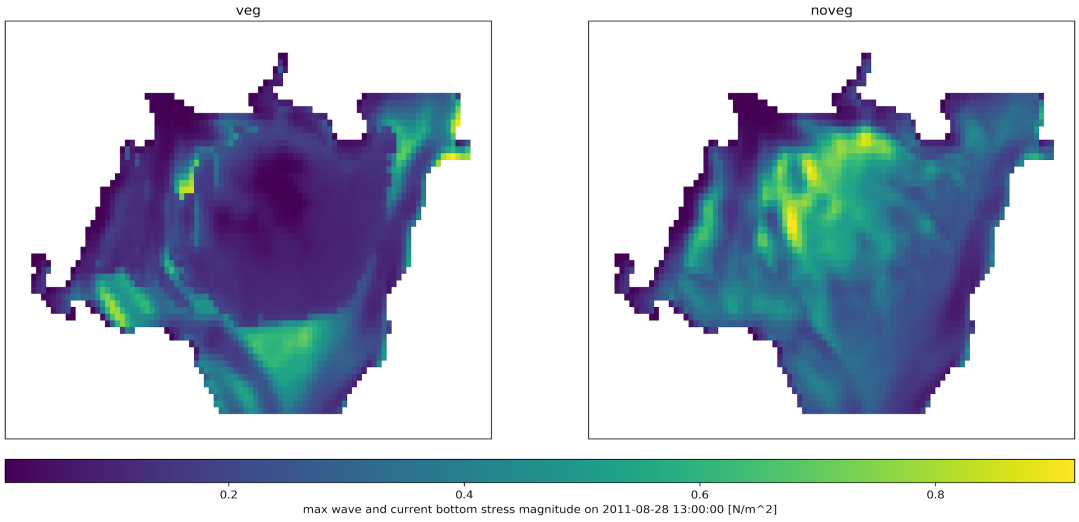

Figure 12: Spatial distribution of maximum wave and current bottom stress magnitude at peak wind conditions on 28 August 2011 at 13:00 during Irene, under vegetative (left) and non-vegetative (right) conditions, from low (blue) to high (yellow).

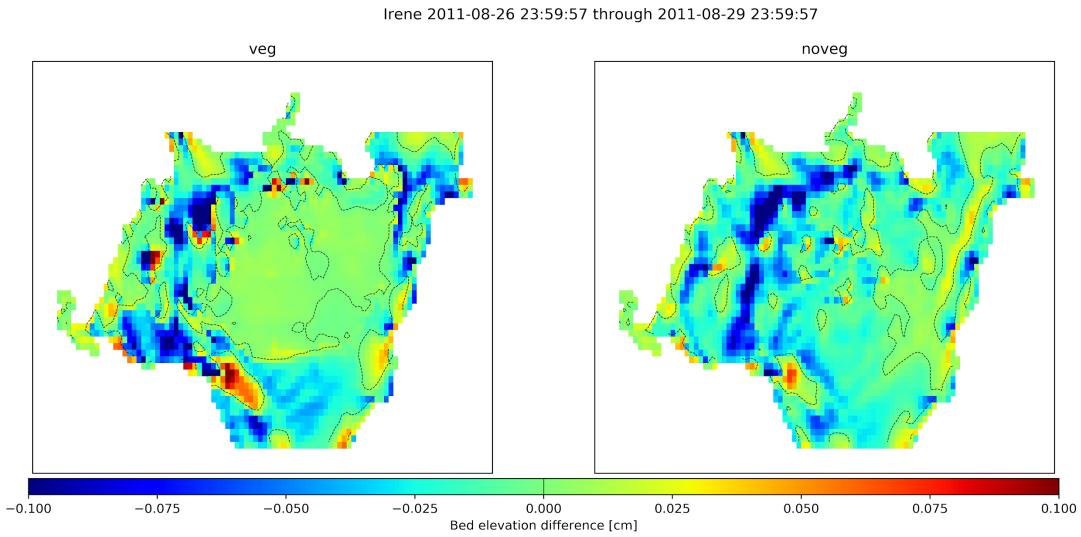

Figure 13: Spatial distribution of the elevation difference (cm) between the final and initial bed thickness over the Irene time period, under vegetative (left) and non-vegetative (right) conditions. Coloring indicates removal of elevation (blues) and addition of elevation (reds) over the time period. A dashed line at zero is included in both panels to indicate the delineation between removal and addition of elevation.

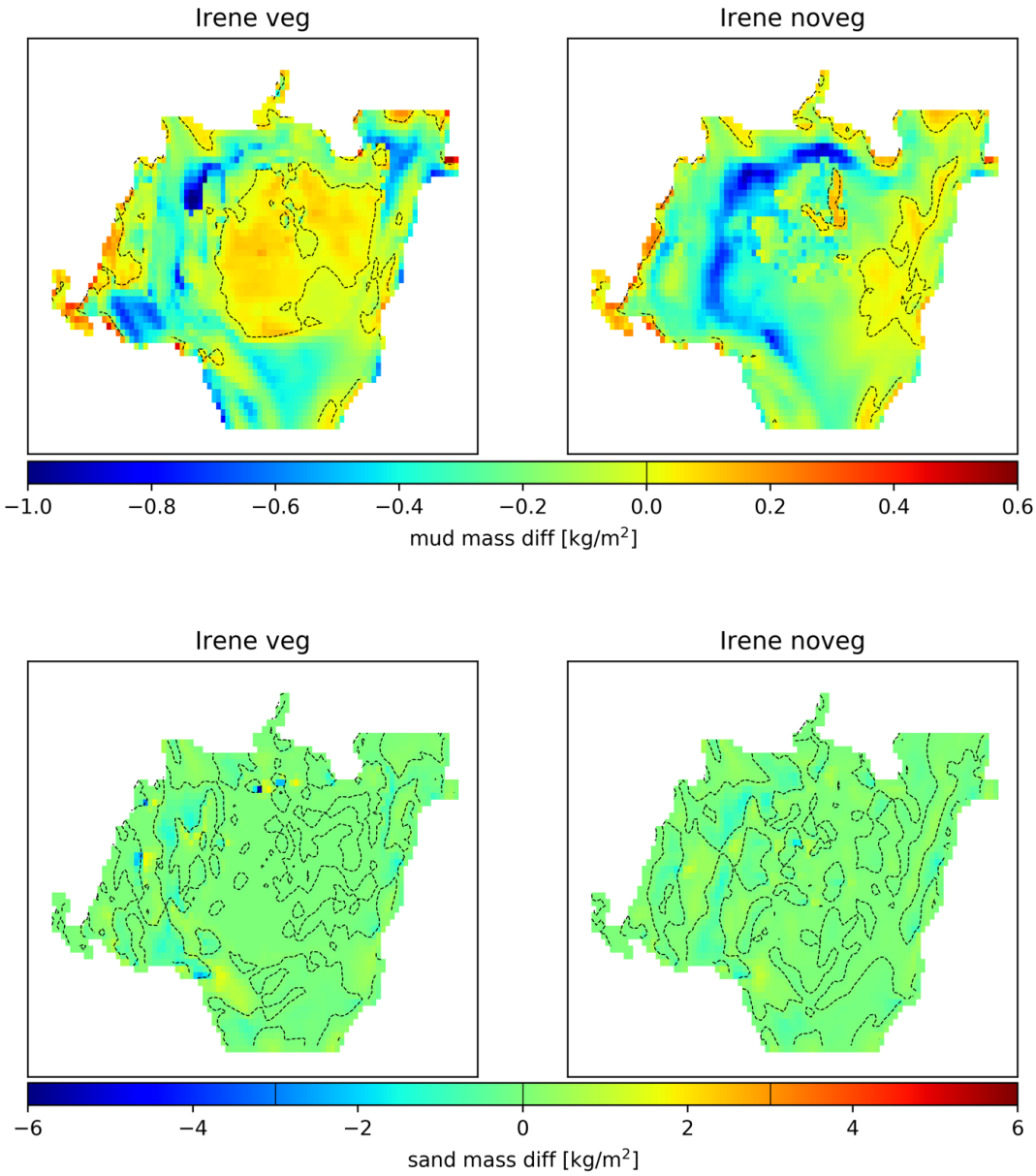

Figure 14: Spatial distribution of the mud mass difference (top two panels) and sand mass difference (kg/m^2) (bottom two panels between the final and initial mass in the bed layer sum over the time period associated with the Irene event, under vegetative (left) and non-vegetative (right) conditions. Coloring indicates removal of mass (blues and greens) and addition of mass (reds) over the time period. A dashed line is included in both panels to indicate the delineation between removal and addition of mass.

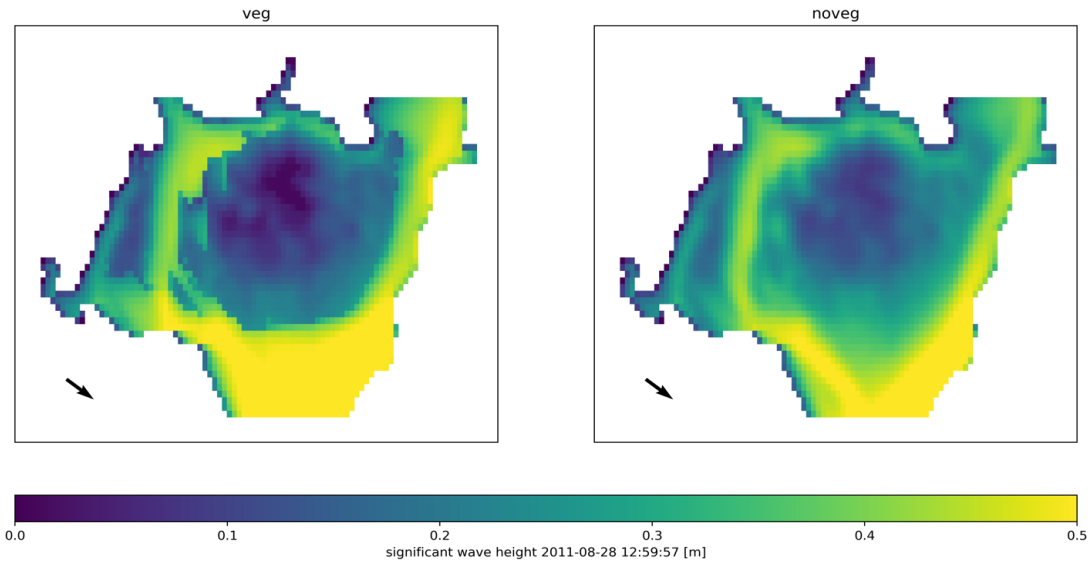

Figure 15: Spatial distribution of significant wave heights (m), smaller (blue) to larger (yellow), during peak winds in Irene, on 29 August 2011 at 13:00, under vegetative (left) and non-vegetative (right) conditions. On each panel an arrow is included to indicate wind direction and speed at the specified time

Tropical Storm (TS) Lee

During TS Lee, the system was heavily influenced by the high river discharge (Figure 16), which resulted in maximum current velocities of 4 m s^{-1} at the mouth of the SR (Figure 17). The impact of vegetation was most obvious in the reduction of the coarse suspended sediment within the vegetation patch (Figure 16). Under both vegetation scenarios, there was significant bottom scour at the mouth of SR (Figure 18). The contrast between channel erosion and flats deposition was greatly increased with vegetation (Figure 18). The amount of sediment that entered the Flats was extremely large and showed a significant amount of deposition (Table 3 and Figure 18). Under vegetative conditions, fine sediment was trapped in the system, mainly within the vegetated region (Figure 19). Some deposition was indicated near the north-east boundary of the system, but this was most likely an artificial response to the model boundary conditions in that region. The coarse material mass difference indicated that

vegetation had an impact on the geospatial patterns of deposition during significant discharge events, only near the main channel (Figure 19).

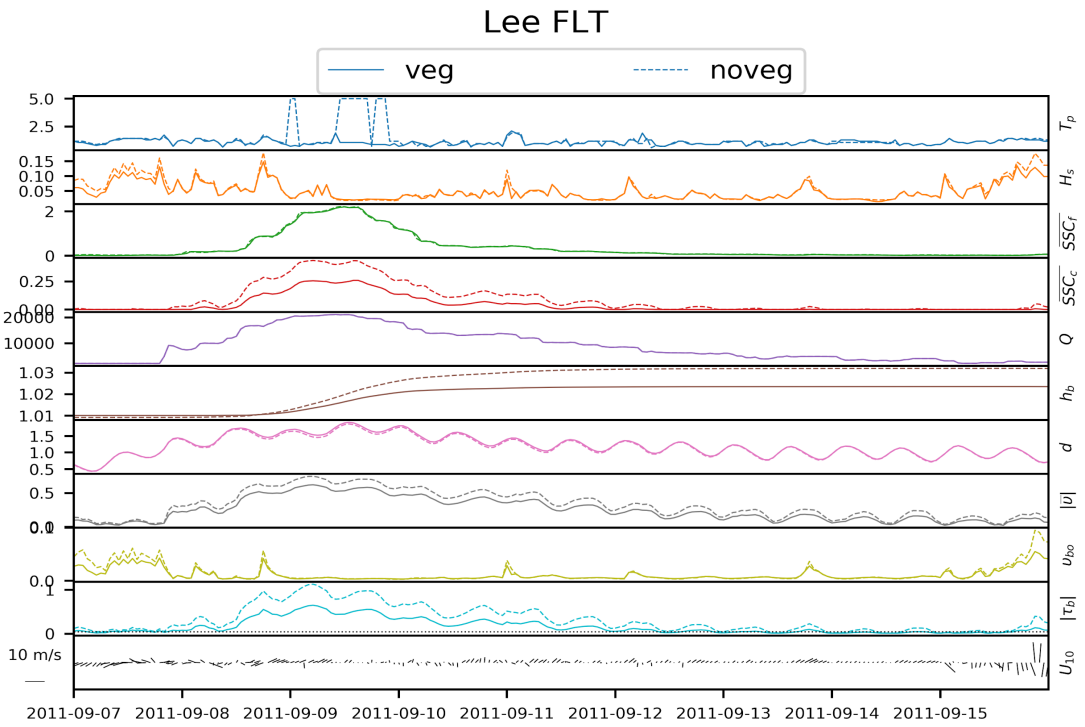

Figure 16: Model prediction summary for FLT during Lee with vegetation (solid) and without vegetation (dashed). From top to bottom the parameters are; T_p - Peak wave period (s), H_s - Significant wave height (m), SSC_f - Depth averaged fine sediment concentration (kg/m^3), SSC_c - Depth averaged coarse sediment concentration (kg/m^3), Q - River discharge (m^3/s), h_b - Bed thickness (m), d - Total water depth (m), $|\bar{v}|$ - Depth averaged current magnitude (m/s),v_{bo} - Wave-induced bottom orbital velocity (m/s), $|\tau_b|$ - Maximum wave and current bottom stress magnitude (N/m^2) with a dotted line indicating the critical shear stress of 0.049 N/m^2, and U_{10} - Wind speed and direction (m/s).

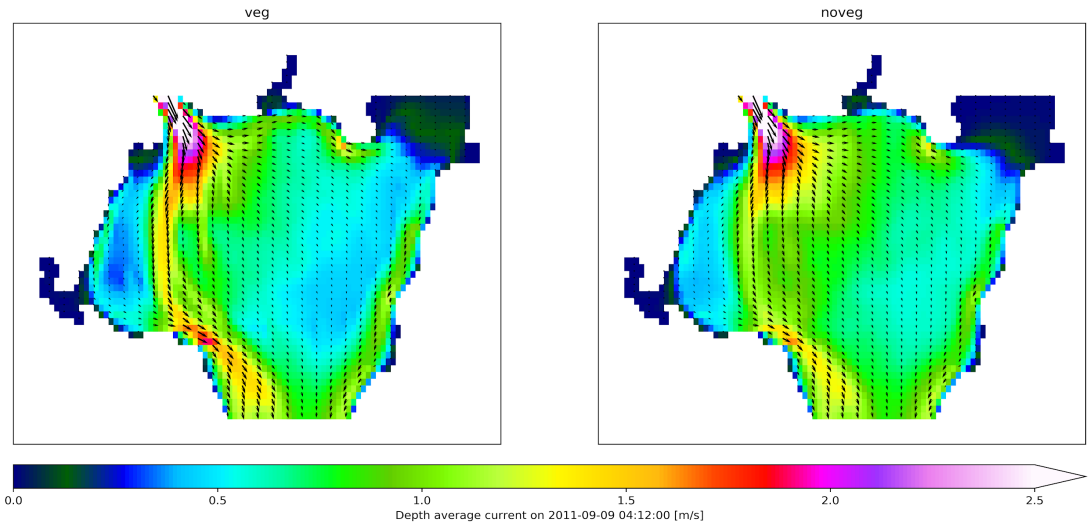

Figure 17: Spatial distribution of depth averaged current speeds (m/s), from low (green) to high (pink/white), with velocity vectors, to indicate direction, during the peak discharge event from Lee, on 9 September 2011 at 04:12, under vegetative (left panel) and non-vegetative (right panel) conditions.

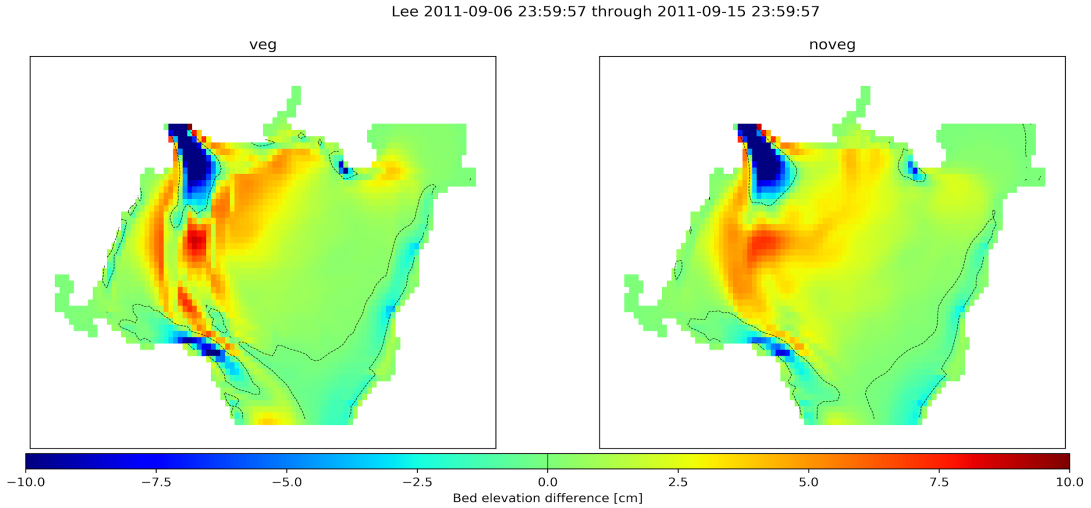

Figure 18: Spatial distribution of the elevation difference (cm) between the final and initial bed thickness over the Lee time period, under vegetative (left) and non-vegetative (right) conditions. Coloring indicates removal of elevation (blues) and addition of elevation (reds) over the time period. A dashed line at zero is included in both panels to indicate the delineation between removal and addition of elevation.

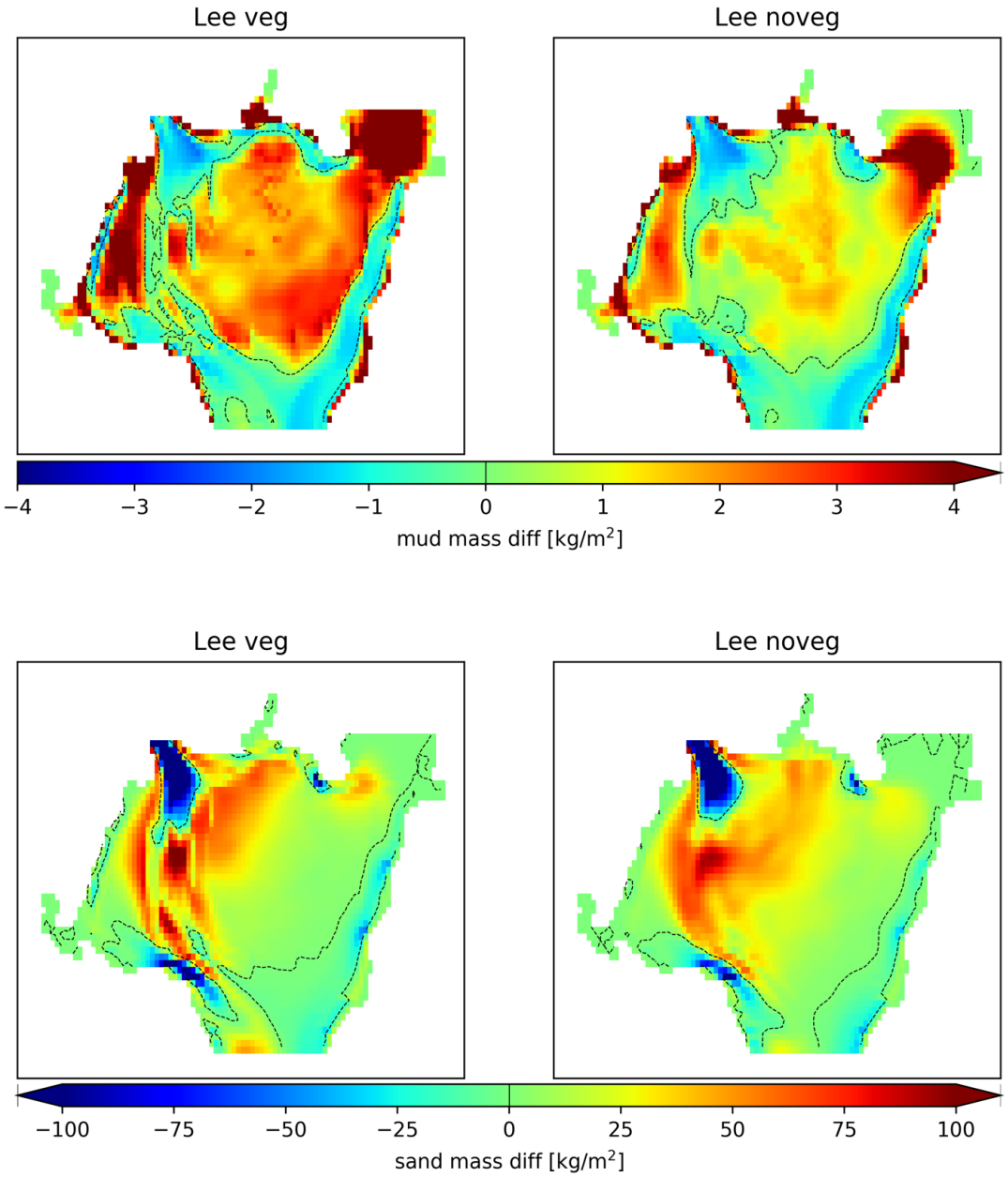

Figure 19: Spatial distribution of the mud mass difference (top two panels) and sand mass difference (kg/m^2) (bottom two panels) between the final and initial mass in the bed layer sum over the time period associated with the Lee event, under vegetative (left) and non-vegetative (right) conditions. Coloring indicates removal of mass (blues and greens) and addition of mass (reds) over the time period. A dashed line is included in all panels to indicate the delineation between removal and addition of mass.

Post-Lee

During the post-Lee period, river discharge averaged 1,914 ± 669 m^3 s^{-1}. There was a wind event that peaked on 20 Oct 2011 with 10.5 m s^{-1} wind velocity (Figure 20). Significant wave heights increased due to higher wind speeds, but they were smaller

within the vegetated patch (Figure 20 and Figure 26). Similar to the Irene event, vegetation reduced the wave and current bottom-stress magnitude (Figure 21). However, the peak wind velocity was 5 m s^{-1} lower than the Irene event, resulting in lower overall bottom stresses (Figure 20). Suspended coarse-sediment concentrations increased at the beginning of the pulses of river discharge and enhanced wave activity (Figure 20), which was enhanced without vegetation (Figure 22). The fine material increase aligned well with the wind events under both vegetative and non-vegetative conditions (Figure 20). The change in bed elevation showed both erosional and depositional patterns at the mouth of the SR with little differences between the vegetative and non-vegetative conditions (Figure 23). The change in mass of the fine sediment class showed there was removal from the south-east region, on the edge of the vegetation patch, which was enhanced under vegetative conditions (Figure 24). The sediment budget indicates that fine sediment exited the region; this export was accentuated under vegetative conditions. However, in both cases, coarse material was trapped (Table 3). Depth-averaged current velocities were higher in the main channel when vegetation existed, while velocities were more widely distributed in the non-vegetative condition (Figure 25). Significant wave heights during peak winds reached maximum of 0.48 m with clear delineation, via wave height reduction, of vegetation (Figure 26).

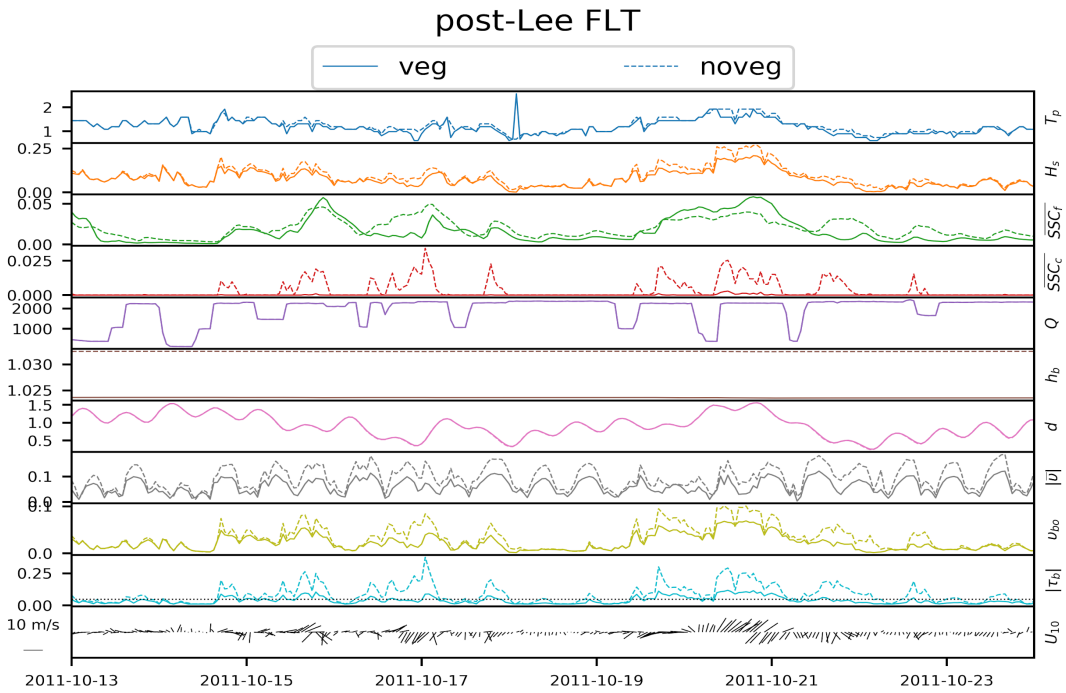

Figure 20: Model prediction summary for FLT during post-Lee with vegetation (solid) and without vegetation (dashed). From top to bottom the parameters are; T_p - Peak wave period (s), H_s - Significant wave height (m), SSC_f - Depth averaged fine sediment concentration (kg/m^3), SSC_c - Depth averaged coarse sediment concentration (kg/m^3), Q - River discharge (m^3/s), h_b - Bed thickness (m), d - Total water depth (m), $|\bar{v}|$ - Depth averaged current magnitude (m/s), v_{bo} - Wave-induced bottom orbital velocity (m/s), $|\tau_b|$ - Maximum wave and current bottom stress magnitude (N/m^2) with a dotted line indicating the critical shear stress of 0.049 N/m^2, and U_{10} - Wind speed and direction (m/s).

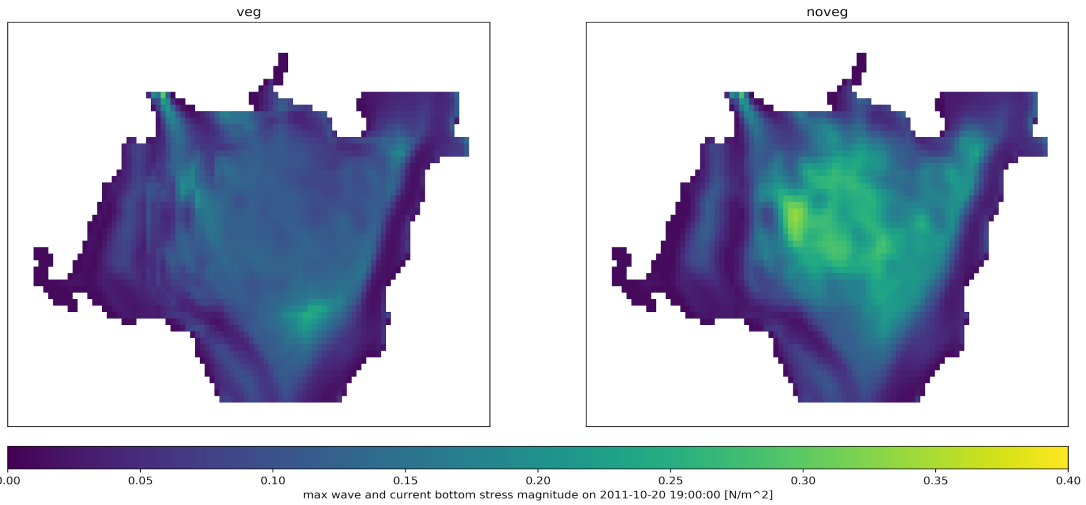

Figure 21: Spatial distribution of maximum wave and current bottom stress magnitude at peak wind conditions on 20 October 2011 at 19:00 during post-Lee, under vegetative (left) and non-vegetative (right) conditions, from low (blue) to high (yellow).

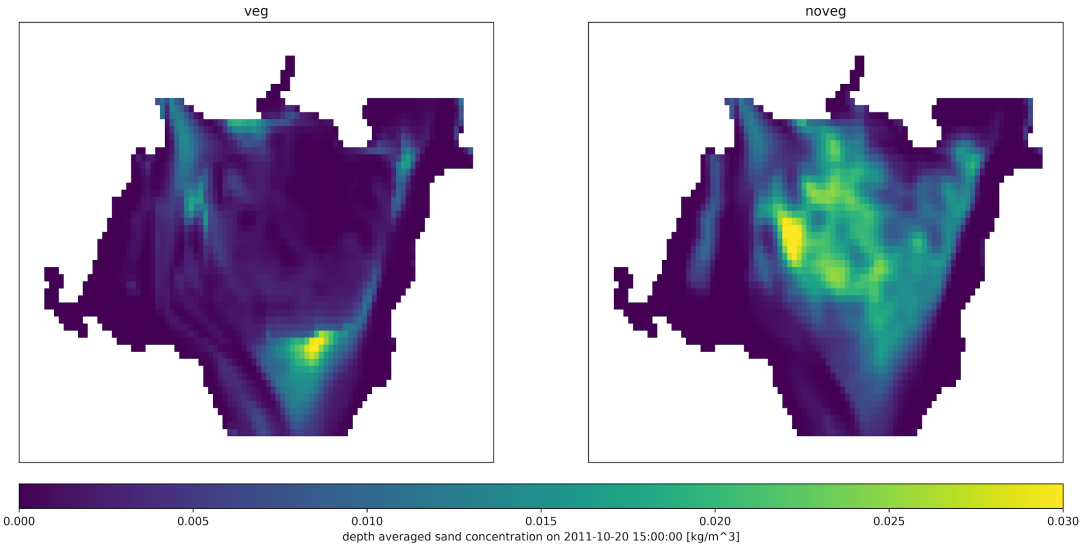

Figure 22: Spatial distribution of the depth averaged concentration of sand (kg/m^3), from low (blue) to high (yellow), during the peak wind event, post-Lee, on 20 October 2011 at 15:00 under vegetative (left) and non-vegetative conditions (right).

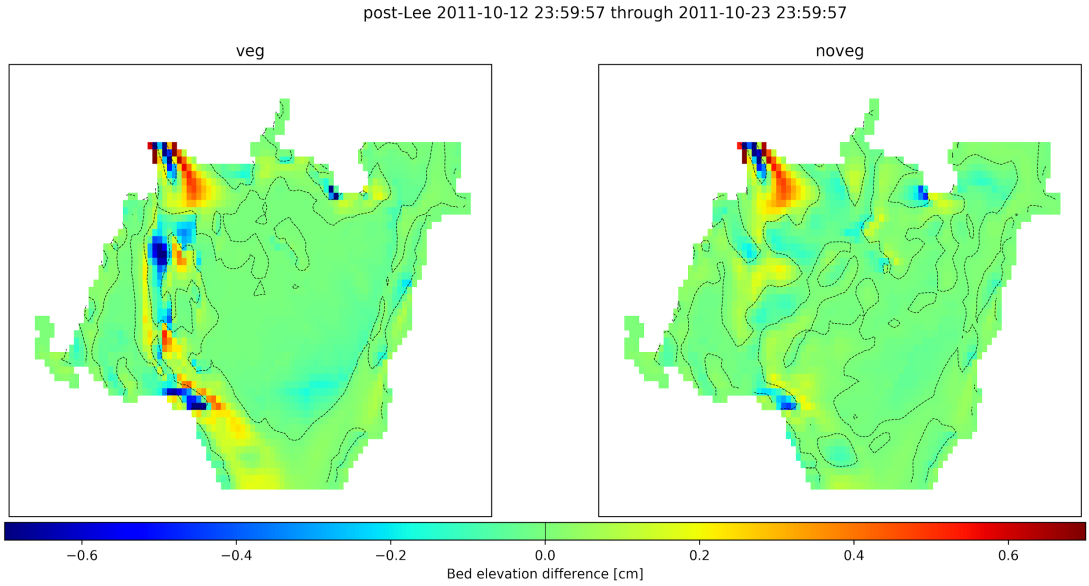

Figure 23: Spatial distribution of the elevation difference (cm) between the final and initial bed thickness over the post-Lee time period, under vegetative (left) and non-vegetative (right) conditions. Coloring indicates removal of elevation (blues) and addition of elevation (reds) over the time period. A dashed line at zero is included in both panels to indicate the delineation between removal and addition of elevation.

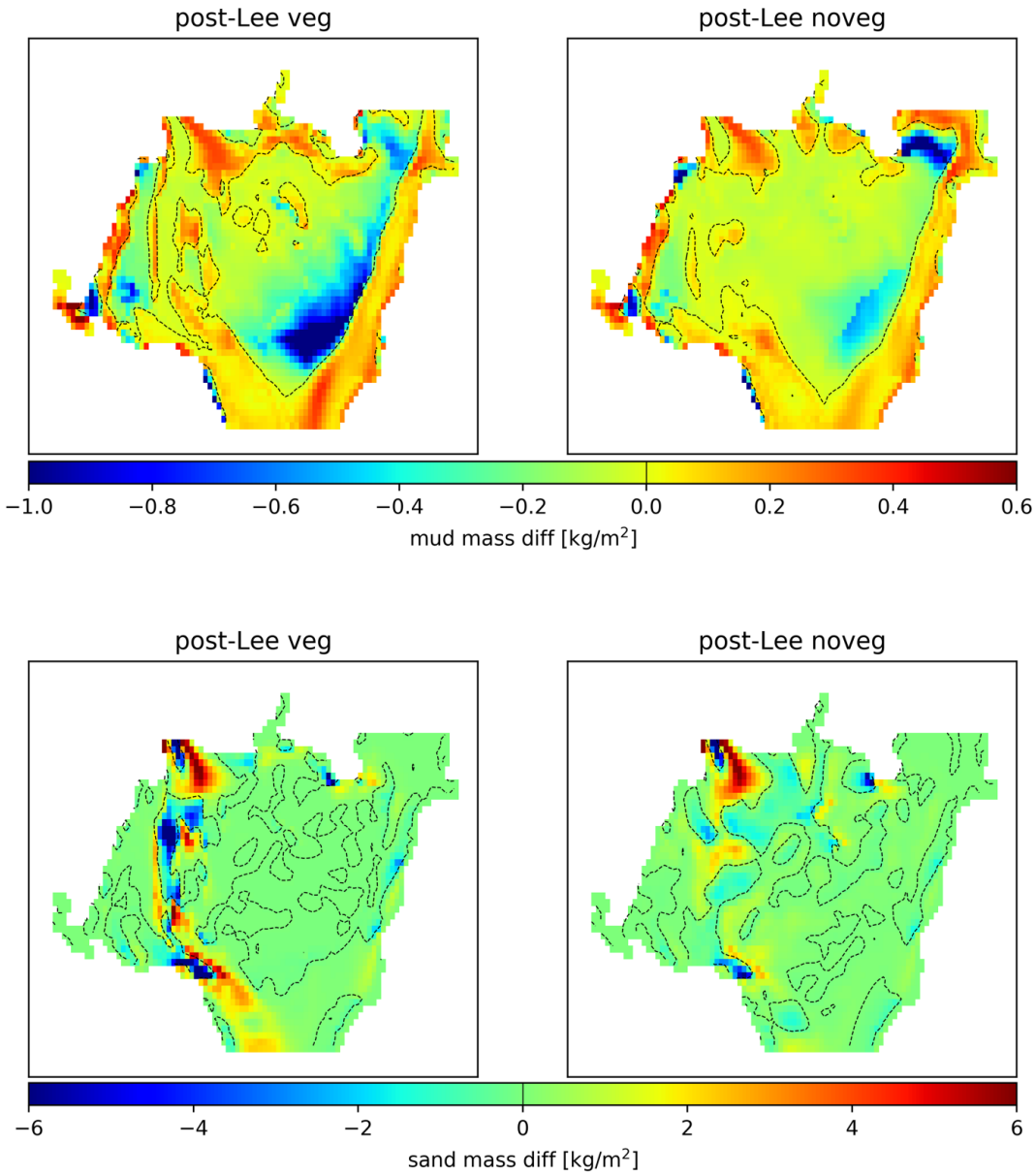

Figure 24: Spatial distribution of the mud mass difference (top two panels) and sand mass difference (kg/m^2) (bottom two panels between the final and initial mass in the bed layer sum over the time period associated with Post Lee, under vegetative (left) and non-vegetative (right) conditions. Coloring indicates removal of mass (blues and greens) and addition of mass (reds) over the time period. A dashed line is included in both panels to indicate the delineation between removal and addition of mass.

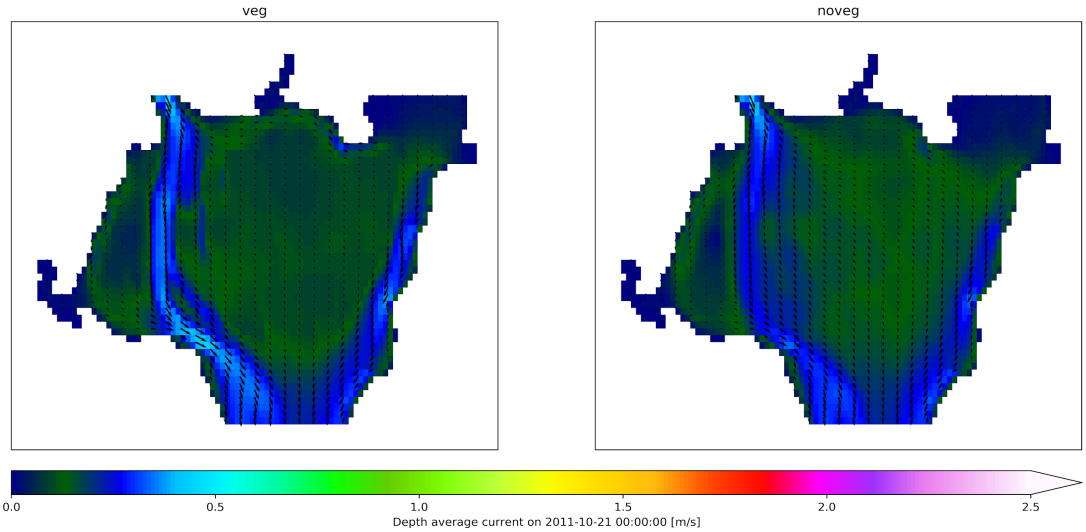

Figure 25: Spatial distribution of depth averaged current speeds (m/s), from low (green) to high (pink/white), with velocity vectors, to indicate direction, during peak current speeds from post-Lee, on 21 October 2011 at 00:00, under vegetative (left panel) and non-vegetative (right panel) conditions.

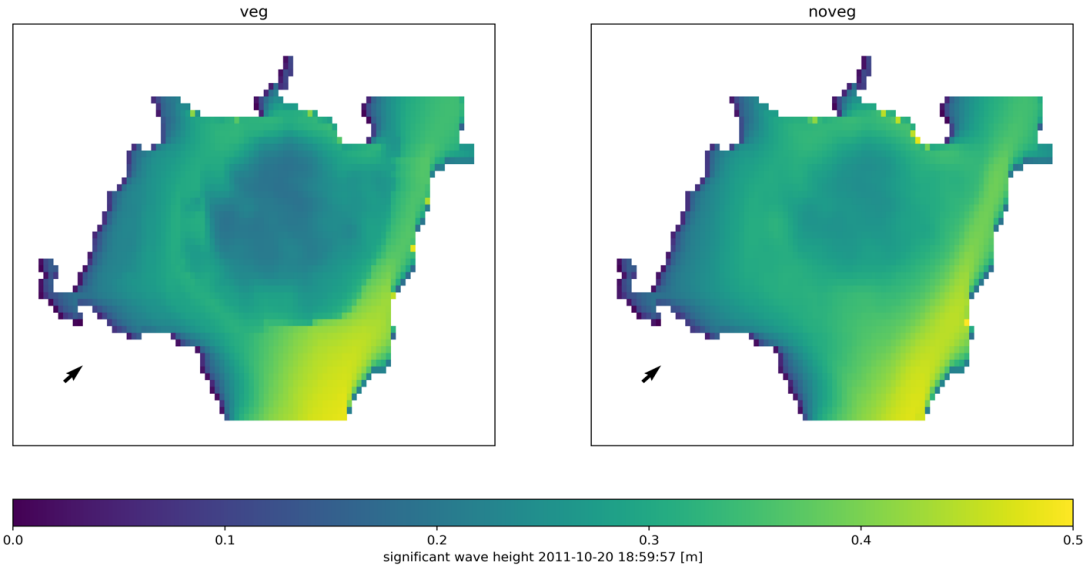

Figure 26: Spatial distribution of significant wave heights (m), smaller (blue) to larger (yellow), during peak winds in post-Lee, on 20 October 2011 at 19:00, under vegetative (left) and non-vegetative (right) conditions. On each panel an arrow is included to indicate wind direction and speed at the specified time.

DISCUSSION

The impacts of vegetation on sediment distribution in the Chesapeake Bay are widely cited as a critical piece of Bay ecosystem dynamics (Gurbisz and Kemp, 2014; Kemp et al., 2005; Russ and Palinkas, 2018). In this study, the COAWST modeling system effectively recreated the physical environment (i.e. currents and wave heights) of

an extremely dynamic bay-head delta system and its response to storm forcing at a high resolution (Figure 5 and Figure 6). The following sections examine its response to storm events, focusing on the role of vegetation and event timing.

Event responses with vegetation

Under normal vegetated conditions, the model indicated a dominance of riverine and tidal processes, with current speeds increasing in the main channel during ebb tide that were enhanced by vegetation (Figure 8). This generated a net export of fine sediment (Table 3), which is primarily due to the resuspension of fine material from the bed layer (Figure 10). However, vegetation plays a role in the geospatial patterns of that removal, focusing it on the main channel (Figure 9 and Figure 10), in part due to the enhanced current speeds (Figure 8 and Figure 10) in these regions, allowing the fine material to be resuspended (Bouma et al., 2007; Cotton et al., 2006; Fisk et al., 1954; Russ and Palinkas, 2018; Wright, 1977). In contrast, coarse material was deposited since current velocities were relatively low (Figure 8), and the settling velocity of coarse material was high (Table 2) (Table 3).

The two periods that had enhanced wind velocities ("Irene" and "Post-Lee") showed an increase in wave heights (Figure 11 and Figure 20), which were dampened by vegetation (Figure 15 and Figure 26). Under high-wave conditions, fine material was exported, but coarse material was deposited, which agrees with the suggestion that some bottom sediments are highly resuspendible (Table 3; Gurbisz et al., 2016). However, there were other physical factors that resulted in differences between events. The Irene wind event was longer-lived with stronger peak wind velocities, which resulted in larger wave heights (Figure 11 and Figure 15), leading to deposition of fine material over the

vegetated region (Figure 14). This agreed with previous studies based on observations during Irene and other events (Palinkas et al., 2014; Sanford, 2008, 1994; Ward et al., 1984). In the Post-Lee period, maximum wind speeds were ~5 m s^{-1} lower but river discharge was higher (Figure 11 and Figure 20), delivering more suspended sediment than Irene (Table 3). Coupling this available sediment with lower energy that allows deposition of coarse material, there is enhanced entrapment of coarse material (Table 3 and Figure 24) that results in a nearly seven-fold increase near the mouth of SR during Post-Lee compared to Irene (Figure 23 and Figure 13).

During large discharge events, the system was completely dominated by riverine dynamics and thus enhanced current velocities (Figure 17), which far exceeded those during other time periods (e.g. 4 m s^{-1} versus 0.5 m s^{-1} under typical conditions). This massive river discharge leads to significant sediment import on par with previous estimations of $6x10^6$ tons (Cheng et al., 2013; Hirsch, 2012; Palinkas et al., 2014), and export from the region. Interestingly, this is the only event which has more import than export of both classes of sediment, resulting in deposition of sediment into the bed layer across a wide swath of the region (Figure 18 and Table 3) which agrees with the geomorphology of bay-head delta development (Dalrymple et al., 1992). The geospatial patterns of deposition are clearly influenced by the presence of vegetation (Figure 19), which modulates current speeds around the vegetation and into the main channel, enhances deposition of fine material (Figure 19), and increases current speeds in the main channel. This limits the deposition of coarse material in the channel while enhancing deposition along the banks in vegetated regions (Figure 17 and Figure 19). Due to

extremely high current velocities at the SR mouth (Figure 17), a significant amount of the bed layer is removed (Figure 18) further enhancing channel development.

Comparing events and removal of vegetation

Evaluating the different time periods, we have shown that that the dynamics are significantly different among events and that timing is crucial to their impact, especially regarding the amount of sediment entering CB (Table 3). Under typical conditions, fine material is eroded and transported to the rest of CB; however, the amounts of sediment are relatively minimal in comparison to wind and discharge-driven events. During massive discharge events, large amounts of sediment are deposited over the region; notably, this is the only time when fine sediment stays in the system. Interestingly, under all events (excluding non-vegetative "Before Irene"), coarse material is retained within the system, hence the need for dredging of the channel (Nichols et al., 1990; Orth et al., 2010).

Evaluating the impacts of vegetation helps address the hypothesis that the existence of plants over the region plays a critical role in modulating the flow and sediment transport to the rest of CB by reducing current speeds over the Flats, therefore enhancing deposition. In all events with vegetation, current speeds in the channel increased from the additional flow resistance of the SAV, increasing current-induced bottom stresses (Figure 17 - current panels). This enhances erosion within the channel and provides a pathway for suspended sediment to be shunted around the Flats and into CB (Luhar et al., 2008).

During typical low energy conditions, when vegetation was removed from the system, there was removal of fine sediment mass from the shallow Flats region (Figure

10), primarily due to the exposure of the bed layer to enhanced current velocities (Figure 8). These enhanced current velocities lead to enhanced bed stresses that suspend both sediment classes but allow fine-sediment concentrations to reach 0.05 kg m^{-3}, which exceeds the threshold for successful SAV growth (0.02 kg m^{-3}; Kemp et al., 2004) (Figure 7). In comparison, suspended sediment in the vegetative conditions approached zero kg m^{-3} (Figure 7), highlighting the ability of SAV to reduce SSC to further facilitate its growth. There is some indication that, under non-vegetative conditions, coarse material is exported from the system (Table 3); however, there is no clear indication as to the geospatial pattern of that removal (Figure 10), and the total amount exported is minimal compared to the other events in this study.

During significant discharge events, vegetation can lead to nearly twice as much fine sediment being deposited in the region, whereas coarse material experiences some decline in the amount of deposition. This indicates that the shunting of water through the main channel by the vegetation can transport some of the coarse material out of the region. However, discharge events result in significant net sediment deposition as similarly observed by Ward et al. (1984), López and García (2001), Russ and Palinkas (2018), and others.

Under wind-driven events, vegetation both enhanced and reduced the retainment of fine sediments within the region, depending on specific characteristics of the event. Vegetation clearly plays a role in the deposition and erosion of material for these two time periods (Irene and post-Lee) (Table 3). During Irene, less fine material was removed from the system under vegetative conditions, indicating that the fine sediment trapped by

vegetation was allowed to transit through the region into the CB when vegetation was absent (Table 3).

Holistically, under vegetative conditions there is less fine material removed during typical and Irene periods and a significant amount deposited during Lee (Table 3). As previously stated, this makes more fine material available for transport out of the system during Post-Lee. However, under non-vegetative conditions there is increased removal of fine sediment during typical and Irene periods and less deposition during Lee (Table 3), reducing the amount of sediment available for transport out during Post-Lee. This leads to the conclusion that the sediment dynamics in the system are highly dependent on the composition of the sediment bed layer leading up to an event with indications that SAV can act as temporary storage of fine sediments.

Temporary storage of fine sediment

The post-Lee and Irene events provide the opportunity to compare similar wind-driven events and investigate the potential role of the sediment dynamics proceeding each event. While sediment transport during both events was primarily driven by wind-wave resuspension (Figure 27), fines were deposited during Irene but eroded post-Lee. We propose that event timing can explain this difference. Specifically, there is a significant amount of deposition of fine material (Figure 14, Figure 19 – top panels, Table 3) prior to the post-Lee event from TS Lee, which contributed up to 4 kg m^{-2} of fine material, presumably in the surface layer and thus available for potential resuspension later on. Since the primary physical driver between the end of Lee and the beginning of post-Lee is river discharge (Figure 2), and that region is somewhat protected by the upstream vegetation (Figure 1), the fine material on the surface remains available for resuspension.

When the region experiences the wind event from post-Lee, that fine material is then resuspended and eroded away. In comparison, Irene essentially only had the surface layer of fine material as initialized in the sediment-bed model available for removal (with some minor removal during "before Irene" 0.1 kg m^{-2}). Therefore, the amount of removal in that region is significantly less, 0.6 kg m^{-2} compared to >1 kg m^{-2}.

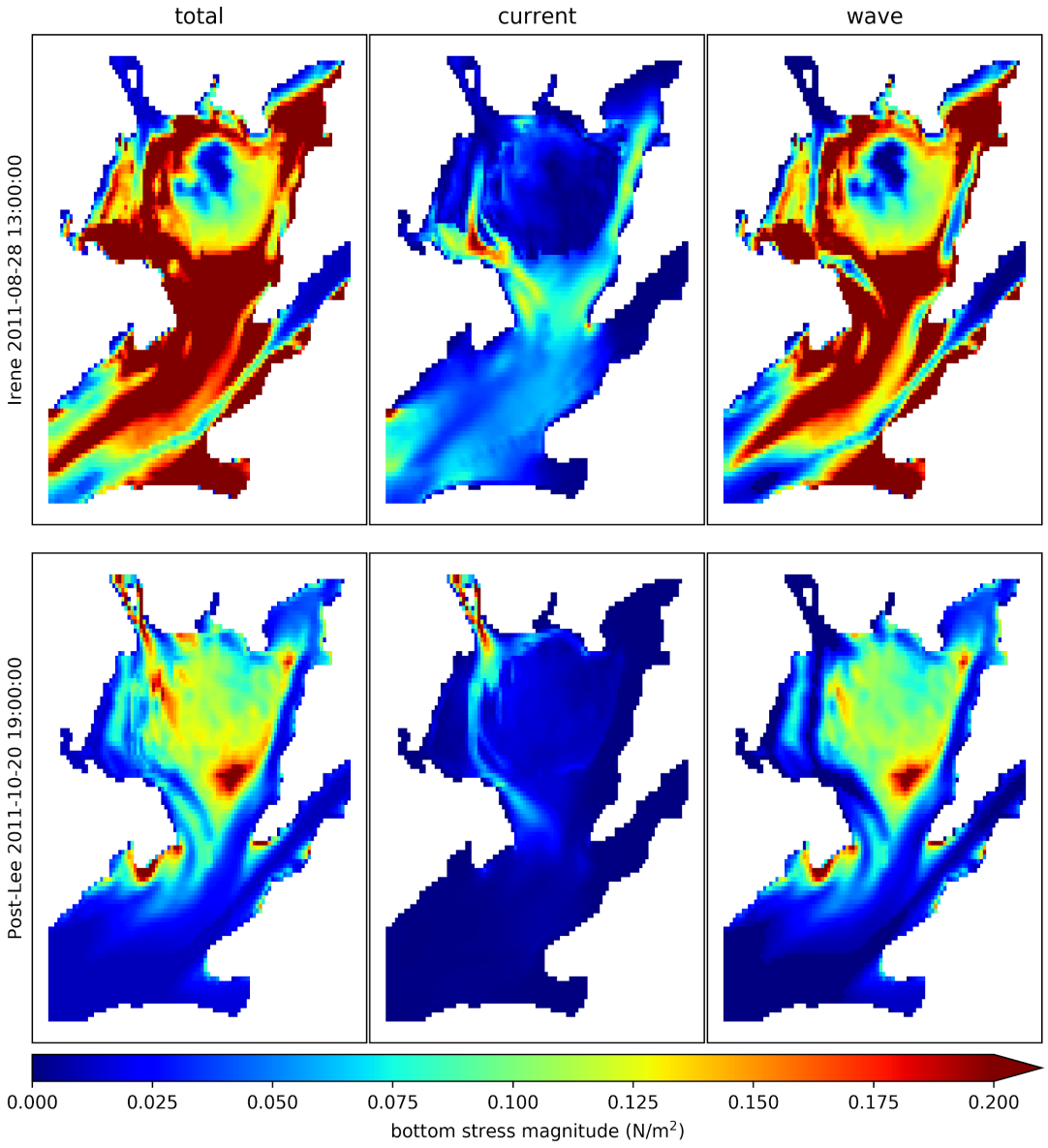

Figure 27: Spatial distribution of total bottom stress magnitude (left panels), current induced bottom stress magnitude (center panels), and wave induced bottom stress magnitude (right panels) at peak wind conditions on during Irene (top panels) and Post-Lee (bottom panels).

The conclusion we gather from these interactions is that SAV over the Flats acts as temporary storage of fine suspended sediment entering CB from the SR. One of the major detriments of fine suspended sediments in CB is its impact on water quality (Langland and Cronin, 2003). Specifically, it reduces the water clarity which impacts SAV further downstream and could lead to reduced SAV populations. Sediment storage also prevents particle-attached nutrients from being transported to CB; seasonal cycles in this storage due to seasonal SAV presence/absence further benefits CB by altering the timing of nutrient delivery. For example, if a significant discharge event occurs in summer or early fall (e.g. TS Lee), this storage can prevent downstream transport of nutrients at a time of enhanced biological productivity. The subsequent release of this material during the winter, when there is less biological activity, from SAV dieback and/or resuspension from winter storms would have much less impact to CB water quality (Bayley et al., 1978; Gurbisz and Kemp, 2014).

Future work

Although the model performed extremely well when attempting to recreate Figure 8 from Gurbisz et al. (2016), the depth-averaged suspended-sediment concentrations from the model at the same locations as the turbidity observations indicated a smaller resuspension event at the FLT station during post-Lee. As shown in Figure 28, the model does a good job matching the rapid increase in suspended material during Lee and even during Irene, but it misses the post-Lee event within the bed. There are a wide range of possibilities for this failure, but mostly likely the bed model needs further refinement to accurately suspend particles rather than sequestering them into the bed. As identified in the METHODS, the model is established as three bed layers, with only the upper 1 cm

consisting of an evenly distributed 13% mud. The mud portion in the 1 cm surface layer is not readily available for resuspension within the vegetation as it gets rapidly sequestered into the coarse bed layers below.

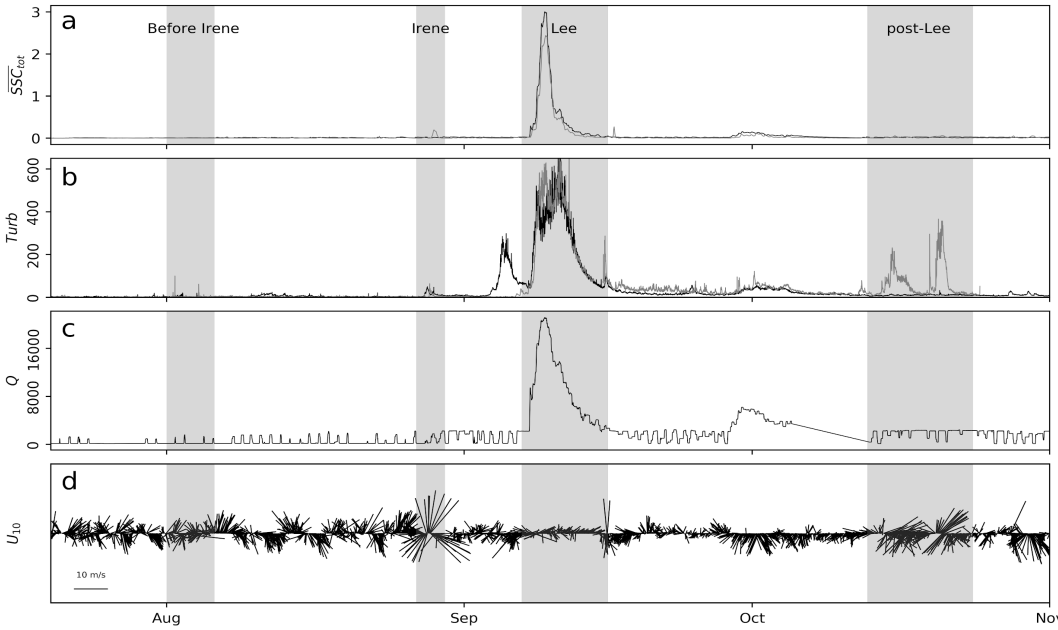

Figure 28: Time series for **a** predicted sum of the depth average sand and mud suspended sediments (kg/m^3) inside (gray) and outside (black) the plant bed, **b** in-situ turbidity (NTU) observations from inside (grey) and outside (black) the plant bed, **c** river discharge observations from the USGS sensor at Conowingo Dam, and **d** wind velocities at the NOAA-NOS CBIBS Susquehanna station.

In addition, further sensitivity experiments on some of the initialization parameters could provide insight into other important conditions for sediment trapping on the Flats. For example, the SAV population was established in this simulation as one species (*V. americana*). However, a wide range of SAV species exist over the region including *Z. marina*, *M. spicatum*, *H. verticillata*, and *H. dubia* (Gurbisz and Kemp, 2014), with each species having their own characteristic plant density, height, thickness, and flexibility. For example, *Z. marina* has a shoot density of 988 shoots m^{-2} and can reach up to 2 m in length (Short et al., 2010), which are both significantly larger than *V. Americana* used in this study. The increase in shoot density and shoot length could result in an increase in the amount of sediment deposited during large discharge events.

Additionally, a less dense species around the edges of the vegetation patch could result in increased shear stresses further inside the vegetation patch, leading to more erosion of fine sediments. Although there is some indication in previous studies that shoot density does not affect the flow in a grass bed exposed to a given ambient current (Fonseca et al., 2019), the current speeds were lower than the peak predicted velocities presented herein.

The change in SAV cover on SF is variable year to year (Gurbisz and Kemp, 2014), with some years showing removal of vegetation. One possibility to appropriately capture the removal of SAV cover within the model would be to include a parameter for critical shear stress for uprooting vegetation (Cabaço et al., 2008; Preen et al., 1995). This would result in changes to the distribution of vegetation, leading to changes in the sediment dynamics during the simulation. This could also facilitate an investigation into the impact of seasonality on how vegetation can modulate sediment transport. If a large discharge event occurred at the beginning of the typical growing season from March to October (Patrick and Weller, 2015), similar timing to Hurricane Agnes in late June 1972, then the shear stress required to uproot the young vegetation would be much lower as the vegetation has not yet established its full root system (Gallegos and Bergstrom, 2005; Moore et al., 1997). In comparison, an event at the end of the typical growing season, similar to TS Lee in early September, could lead to a removal of vegetation due to shear stresses exceeding the uprooting criteria, resulting in significant changes to the sediment dynamics and possibly increasing the amount of sediment removed during the post-Lee wind event.

Broader impacts

This study highlights the dynamic nature of the region, showing that SAV not only enhances deposition of fine sediment but also affects water flow by forcing it through unvegetated channels. This enhanced flow could lead to channel erosion and thus limit the need for channel dredging. However, the current speeds required for enhanced erosion within the channel could exceed critical shear stresses that lead to uprooting of vegetation (Cabaço et al., 2008; Preen et al., 1995), thus distributing the flow to other regions within the bed.

There is evidence that further supports SAV as ecosystem engineers (Jones et al., 1996; Koch, 2001) through the "before Irene" event. This time period indicated that when vegetation does not exist in the region, fine SSC exceeded the threshold for successful SAV survival. However, when vegetation was included, it reduced current speeds enough to facilitate a decrease in fine SSC, thus increasing water clarity, potentially leading to its survival success.

This successful evaluation of the modeling system can lead us to ask more pointed questions about the sedimentary response to SAV at a fluvial-estuarine interface. Some of these questions include: What are the impacts different species of SAV have on sediment deposition? Would it be possible to control the delayed release of fine sediment into the CB to release during non-growing seasons? How does removal (or addition) of portions of a SAV patch impact the sediment dynamics? Does the Beudin et al. (2017) formulation for flexible vegetation result in capturing additional sedimentary components, or would a more simplistic enhanced bottom roughness be sufficient?

CONCLUSION

Submersed aquatic vegetation has a significant impact on sediment transport in the upper Chesapeake Bay (CB). Due to the proximity of vegetated beds to the mouth of the Susquehanna River and the rest of the CB, their capability to modulate sediment has significant impacts on downstream CB water quality. The main objective of this study was to recreate, at a high resolution, the existing environment during storm events and evaluate the potential impacts of vegetation and event timing on sediment transport. Although the sediment bed model needs some refinement, the simulations show an unprecedented level of realism and indicate that the dynamics within the system are temporally variable and geospatially diverse. This work emphasizes the capability of the Flats to act as temporary storage of suspended fine sediments after large discharge events, with Submerged Aquatic Vegetation (SAV) nearly doubling the capacity. There is also further support that SAV act as ecosystem engineers by facilitating an increase in water clarity, supporting their survival. However, the dependence of wind-driven resuspension on the previous sedimentary conditions shows that not only are environmental forcings at the time of occurrence important, but the timing of those events in relation to other environmental forcings can have significant impacts on the system's sedimentary response. Using a tool like this to evaluate the various physical controls within the system can be enormously useful in evaluating potential climate and anthropogenic changes to vegetated bay-head delta systems.

REFERENCES

Barbosa, S.M., Silva, M.E., 2009. Low-frequency sea-level change in Chesapeake Bay: Changing seasonality and long-term trends. Estuar. Coast. Shelf Sci. 83, 30–38. https://doi.org/10.1016/j.ecss.2009.03.014

Bayley, S., Stotts, V.D., Springer, P.F., Steenis, J., 1978. Changes in Submerged Aquatic Macrophyte Populations at the Head of Chesapeake Bay, 1958-1975. Estuaries 1, 171. https://doi.org/10.2307/1351459

Beudin, A., Kalra, T.S., Ganju, N.K., Warner, J.C., 2017. Development of a coupled wave-flow-vegetation interaction model. Comput. Geosci. 100, 76–86. https://doi.org/10.1016/j.cageo.2016.12.010

Booij, N., Ris, R.C., Holthuijsen, L.H., 1999. A third-generation wave model for coastal regions 1. Model description and validation. J. Geophys. Res. Ocean. 104, 7649–7666. https://doi.org/10.1029/98JC02622

Bouma, T.J., van Duren, L.A., Temmerman, S., Claverie, T., Blanco-Garcia, A., Ysebaert, T., Herman, P.M.J., 2007. Spatial flow and sedimentation patterns within patches of epibenthic structures: Combining field, flume and modelling experiments. Cont. Shelf Res. 27, 1020–1045. https://doi.org/10.1016/j.csr.2005.12.019

Cabaço, S., Santos, R., Duarte, C.M., 2008. The impact of sediment burial and erosion on seagrasses: A review. Estuar. Coast. Shelf Sci. https://doi.org/10.1016/j.ecss.2008.04.021

Catling, P., Spicer, K., Biernacki, M., Lovett Doust, J., 1994. The biology of Canadian weeds. 103. Vallisneria americana Michx. Can. J. Plant Sci. 74, 883–897. https://doi.org/10.4141/cjps94-160

Chen, S.-N., Sanford, L.P., Koch, E.W., Shi, F., North, E.W., 2007. A nearshore model to investigate the effects of seagrass bed geometry on wave attenuation and suspended sediment transport. Estuaries and Coasts 30, 296–310. https://doi.org/10.1007/BF02700172

Cheng, P., Li, M., Li, Y., 2013. Generation of an estuarine sediment plume by a tropical storm. J. Geophys. Res. Ocean. 118, 856–868. https://doi.org/10.1002/jgrc.20070

Chesapeake Research Consortium, 1976. The effects of tropical storm Agnes on the Chesapeake Bay system, CRC Public. ed. Johns Hopkins University Press, Baltimore.

Cotton, J.A., Wharton, G., Bass, J.A.B., Heppell, C.M., Wotton, R.S., 2006. The effects of seasonal changes to in-stream vegetation cover on patterns of flow and accumulation of sediment. Geomorphology 77, 320–334. https://doi.org/10.1016/j.geomorph.2006.01.010

Dalrymple, R.W., Zaitlin, B. a, Boyd, R., 1992. Estuarine facies models; conceptual basis and stratigraphic implications. J. Sediment. Res. 62, 1130–1146. https://doi.org/10.1306/D4267A69-2B26-11D7-8648000102C1865D

Davis, F.W., 1985. Historical changes in submerged macrophyte communities of upper Chesapeake Bay. Ecology 66, 981–993. https://doi.org/10.2307/1940560

Dennison, B., Saxby, T., Walsh Bill Dennison, B., Fries, A., Walsh, B., McCollough, C., Michael, B., Naylor, M., Parham, T., Trice, M., Glibert, P., Gurbisz, C., Kemp, M., Palinkas, C., Sanford, L., Fraser, J., Karpanty, S., 2012. Ecological impacts of Hurricane Sandy on Chesapeake & Delmarva Coastal Bays.

Donatelli, C., Ganju, N.K., Fagherazzi, S., Leonardi, N., 2018. Seagrass Impact on Sediment Exchange Between Tidal Flats and Salt Marsh, and The Sediment Budget of Shallow Bays. Geophys. Res. Lett. 45, 4933–4943. https://doi.org/10.1029/2018GL078056

Fisher, A.W., Sanford, L.P., Suttles, S.E., 2015. Wind Stress Dynamics in Chesapeake Bay: Spatiotemporal Variability and Wave Dependence in a Fetch-Limited Environment*. J. Phys. Oceanogr. 45, 2679–2696. https://doi.org/10.1175/JPO-D-15-0004.1

Fisk, H.N., Kolb, C.R., McFarlan, E., Wilbert, L.J., 1954. Sedimentary framework of the modern Mississippi delta [Louisiana]. J. Sediment. Res. 24, 76–99. https://doi.org/10.1306/d4269661-2b26-11d7-8648000102c1865d

Fonseca, M.S., Fourqurean, J.W., Koehl, M.A.R., 2019. Effect of seagrass on current speed: Importance of flexibility vs. shoot density. Front. Mar. Sci. 6. https://doi.org/10.3389/fmars.2019.00376

Gallegos, C.L., Bergstrom, P.W., 2005. Effects of a Prorocentrum minimum bloom on light availability for and potential impacts on submersed aquatic vegetation in upper Chesapeake Bay, in: Harmful Algae. pp. 553–574. https://doi.org/10.1016/j.hal.2004.08.016

Gambi, M., Nowell, A., Jumars, P., 1990. Flume observations on flow dynamics in Zostera marina (eelgrass) beds. Mar. Ecol. Prog. Ser. https://doi.org/10.3354/meps061159

Granata, T.C., Serra, T., Colomer, J., Casamitjana, X., Duarte, C.M., Gacia, E., 2001. Flow and particle distributions in a nearshore seagrass meadow before and after a storm. Mar. Ecol. Prog. Ser. https://doi.org/10.3354/meps218095

Gross, M., Karweit, M., Cronin, W., Schubel, J.R., 1978. Suspended Sediment Discharge of the Susquehanna River to Northern Chesapeake Bay, 1966 to 1976. Estuaries 1, 106–110.

Gurbisz, C., Kemp, W.M., 2014. Unexpected resurgence of a large submersed plant bed in Chesapeake Bay: Analysis of time series data. Limnol. Oceanogr. 59, 482–494. https://doi.org/10.4319/lo.2014.59.2.0482

Gurbisz, C., Kemp, W.M., Sanford, L.P., Orth, R.J., 2016. Mechanisms of Storm-Related Loss and Resilience in a Large Submersed Plant Bed. Estuaries and Coasts 39, 951–966. https://doi.org/10.1007/s12237-016-0074-4

Harris, C.K., Sherwood, C.R., Signell, R.P., Bever, A.J., Warner, J.C., 2008. Sediment dispersal in the northwestern Adriatic Sea. J. Geophys. Res. Ocean. 113.

https://doi.org/10.1029/2006JC003868

Hedström, K.S., 2009. Technical Manual for a Coupled Sea-Ice / Ocean Circulation Model (Version 3). Circulation 158.

Hirsch, R.M., 2012. Flux of Nitrogen, Phosphorus, and Suspended Sediment from the Susquehanna River Basin to the Chesapeake Bay during Tropical Storm Lee, September 2011, as an indicator of the effects of reservoir sedimentation on water quality 17.

Hsu, S.A., Meindl, E.A., Gilhousen, D.B., 1994. Determining the Power-Law Wind-Profile Exponent under Near-Neutral Stability Conditions at Sea. J. Appl. Meteorol. 33, 757–765. https://doi.org/10.1175/1520-0450(1994)033<0757:dtplwp>2.0.co;2

Jones, C.G., Lawton, J.H., Shachak, M., 1996. Organisms as Ecosystem Engineers BT - Ecosystem Management: Selected Readings, in: Ecosystem Management. Springer New York, pp. 130–147. https://doi.org/10.1007/978-1-4612-4018-1_14

Kemp, W.M., Batiuk, R., Bartleson, R., Bergstrom, P., Carter, V., Gallegos, C.L., Hunley, W., Karrh, L., Koch, E.W., Landwehr, J.M., Moore, K.A., Murray, L., Naylor, M., Rybicki, N.B., Stevenson, J.C., Wilcox, D.J., 2004. Habitat Requirements for Submerged Aquatic Vegetation in Chesapeake Bay: Water Quality, Light Regime, and Physical-Chemical Factors. Estuar. Res. Fed. Estuaries 363, 363–377.

Kemp, W.M., Boynton, W.R., Adolf, J.E., Boesch, D.F., Boicourt, W.C., Brush, G., Cornwell, J.C., Fisher, T.R., Glibert, P.M., Hagy, J.D., Harding, L.W., Houde, E.D., Kimmel, D.G., Miller, W.D., Newell, R.I.E., Roman, M.R., Smith, E.M., Stevenson, J.C., 2005. Eutrophication of Chesapeake Bay: historical trends and ecological interactions, MARINE ECOLOGY PROGRESS SERIES Mar Ecol Prog Ser.

Kilbourne, B.F., 2017. Meteorological and surface water observations from the Chesapeake Bay Interpretive Buoy System from 2007-04-25 to 2017-12-31 (NCEI Accession 0159578).

Koch, E.W., 2001. Beyond light: Physical, geological, and geochemical parameters as possible submersed aquatic vegetation habitat requirements. Estuaries. https://doi.org/10.2307/1352808

Komen, G.J., Hasselmann, S., Hasselmann, K., 1984. On the existence of a fully developed wind-sea spectrum. J. PHYS. Ocean. https://doi.org/10.1175/1520-0485(1984)014<1271:oteoaf>2.0.co;2

Kreiling, R.M., Yin, Y., Gerber, D.T., 2007. Abiotic influences on the biomass of Vallisneria americana Michx. In the Upper Mississippi River. River Res. Appl. 23, 343–349. https://doi.org/10.1002/rra.984

Langland, Cronin, 2003. A Summary Report of Sediment Processes in Chesapeake Bay and Watershed.

Lee, S.B., Li, M., Zhang, F., 2017. Impact of sea level rise on tidal range in Chesapeake and Delaware Bays. J. Geophys. Res. Ocean. 122, 3917–3938. https://doi.org/10.1002/2016JC012597

Liu, X., Wang, M., 2014. River runoff effect on the suspended sediment property in the upper Chesapeake Bay using MODIS observations and ROMS simulations. J. Geophys. Res. Ocean. 119, 8646–8661. https://doi.org/10.1002/2014JC010081

López, F., García, M.H., 2001. Mean Flow and Turbulence Structure of Open-Channel Flow through Non-Emergent Vegetation. J. Hydraul. Eng. 127, 392–402. https://doi.org/10.1061/(ASCE)0733-9429(2001)127:5(392)

Lovett-Doust, J., Laporte, G., 1991. Population sex ratios, population mixtures and fecundity in a clonal dioecious macrophyte, Vallisneria americana. J. Ecol. 79, 477–489. https://doi.org/10.2307/2260727

Luhar, M., Rominger, J., Nepf, H., 2008. Interaction between flow, transport and vegetation spatial structure. Environ. Fluid Mech. 8, 423–439. https://doi.org/10.1007/s10652-008-9080-9

Madsen, O.S., 1995. Spectral wave-current bottom boundary layer flows, in: Proceedings of the Coastal Engineering Conference. ASCE, pp. 384–398. https://doi.org/10.1061/9780784400890.030

Moore, K.A., Wetzel, R.L., Orth, R.J., 1997. Seasonal pulses of turbidity and their relations to eelgrass (Zostera marina L.) survival in an estuary. J. Exp. Mar. Bio. Ecol. 215, 115–134. https://doi.org/10.1016/S0022-0981(96)02774-8

Morin, J., Leclerc, M., Secretan, Y., Boudreau, P., 2000. Integrated two-dimensional macrophytes-hydrodynamic modeling. J. Hydraul. Res. 38, 163–172. https://doi.org/10.1080/00221680009498334

National Centers for Environmental Information, 2017. NOAA NOS Estuarine Bathymetry - Chesapeake Bay (M130). https://doi.org/10.7289/V5ZK5F0X

Nichols, M., Diaz, R.J., Schaffner, L.C., 1990. Effects of hopper dredging and sediment dispersion, chesapeake bay. Environ. Geol. Water Sci. 15, 31–43. https://doi.org/10.1007/BF01704879

Orth, R.J., Williams, M.R., Marion, S.R., Wilcox, D.J., Carruthers, T.J.B., Moore, K.A., Kemp, W.M., Dennison, W.C., Rybicki, N., Bergstrom, P., Batiuk, R.A., 2010. Long-Term Trends in Submersed Aquatic Vegetation (SAV) in Chesapeake Bay, USA, Related to Water Quality. Estuaries and Coasts 33, 1144–1163. https://doi.org/10.1007/s12237-010-9311-4

Palinkas, C.M., Halka, J.P., Li, M., Sanford, L.P., Cheng, P., 2014. Sediment deposition from tropical storms in the upper Chesapeake Bay: Field observations and model simulations. Cont. Shelf Res. 86, 6–16. https://doi.org/10.1016/j.csr.2013.09.012

Patrick, C., Weller, D., 2015. Interannual variation in submerged aquatic vegetation and its relationship to water quality in subestuaries of Chesapeake Bay 537, 121–135. https://doi.org/10.3354/meps11412

Peterson, C.H., Luettich, R.A., Micheli, F., Skilleter, G.A., 2004. Attenuation of water flow inside seagrass canopies of differing structure. Mar. Ecol. Prog. Ser. https://doi.org/10.3354/meps268081

Preen, A.R., Lee Long, W.J., Coles, R.G., 1995. Flood and cyclone related loss, and

partial recovery, of more than 1000 km2 of seagrass in Hervey Bay, Queensland, Australia. Aquat. Bot. 52, 3–17. https://doi.org/10.1016/0304-3770(95)00491-H

Redfield, A.C., 1972. Development of a New England Salt Marsh. Ecol. Monogr. 42, 201–237. https://doi.org/10.2307/1942263

Russ, E.R., Palinkas, C.M., 2018. Seasonal-Scale and Decadal-Scale Sediment-Vegetation Interactions on the Subaqueous Susquehanna River Delta, Upper Chesapeake Bay. Estuaries and Coasts 41, 2092–2104. https://doi.org/10.1007/s12237-018-0413-8

Sand-jensen, K., 1998. Influence of submerged macrophytes on sediment composition and near-bed flow in lowland streams. Freshw. Biol. 39, 663–679. https://doi.org/10.1046/j.1365-2427.1998.00316.x

Sanford, L.P., 2008. Modeling a dynamically varying mixed sediment bed with erosion, deposition, bioturbation, consolidation, and armoring. Comput. Geosci. 34, 1263–1283. https://doi.org/10.1016/j.cageo.2008.02.011

Sanford, L.P., 1994. Wave-Forced Resuspension of Upper Chesapeake Bay Muds. Estuaries 17, 148. https://doi.org/10.2307/1352564

Sanford, L.P., Suttles, S.E., Halka, J.P., 2007. Reconsidering the Physics of the Chesapeake Bay Estuarine Turbidity Maximum. Estuaries 24, 655. https://doi.org/10.2307/1352874

Schubel, J.R., Pritchard, D.W., 1986. Responses of Upper Chesapeake Bay to Variations in Discharge of the Susquehanna River. Source Estuaries UTC Estuaries 946, 236–24919. https://doi.org/10.2307/1352096

Shchepetkin, A.F., McWilliams, J.C., 2005. The regional oceanic modeling system (ROMS): a split-explicit, free-surface, topography-following-coordinate oceanic model. Ocean Model. 9, 347–404. https://doi.org/10.1016/J.OCEMOD.2004.08.002

Short, F.T., Carruthers, T.J.R., Waycott, M., Kendrick, G.A., Fourqurean, J.W., Callabine, A., Kenworthy, W.J., Dennison, W.C., 2010. Zostera marina. The IUCN Red List of Threatened Species 2010: e.T153538A4516675. IUCN Red List Threat. Species 8235. https://doi.org/10.2305/IUCN.UK.2010-3.RLTS.T153538A4516675.en

Skamarock, C., Klemp, B., Dudhia, J., Gill, O., Barker, M., Wang, W., Powers, G., 2005. A Description of the Advanced Research WRF Version 2. https://doi.org/10.5065/D6DZ069T

Walter, R.C., Merritts, D.J., 2008. Natural streams and the legacy of water-powered mills. Science (80-.). https://doi.org/10.1126/science.1151716

Ward, L.G., Michael Kemp, W., Boynton, W.R., 1984. The influence of waves and seagrass communities on suspended particulates in an estuarine embayment. Mar. Geol. 59, 85–103. https://doi.org/10.1016/0025-3227(84)90089-6

Warner, J.C., Armstrong, B., He, R., Zambon, J.B., 2010. Development of a Coupled Ocean-Atmosphere-Wave-Sediment Transport (COAWST) Modeling System. Ocean Model. 35, 230–244. https://doi.org/10.1016/j.ocemod.2010.07.010

Warner, J.C., Geyer, W.R., Lerczak, J.A., 2005. Numerical modeling of an estuary: A comprehensive skill assessment. J. Geophys. Res. C Ocean. 110, 1–13. https://doi.org/10.1029/2004JC002691

Warner, J.C., Sherwood, C.R., Signell, R.P., Harris, C.K., Arango, H.G., 2008. Development of a three-dimensional, regional, coupled wave, current, and sediment-transport model. Comput. Geosci. 34, 1284–1306. https://doi.org/10.1016/j.cageo.2008.02.012

Wessel, P., Smith, W.H.F., 1996. A global, self-consistent, hierarchical, high-resolution shoreline database. J. Geophys. Res. Solid Earth 101, 8741–8743. https://doi.org/10.1029/96JB00104

Williams, K.F., Reed, L.A., 1972. Appraisal of stream sedimentation in the Susquehanna River basin. https://doi.org/10.3133/wsp1532F

Wright, L.D., 1977. Sediment transport and deposition at river mouths: A synthesis. Bull. Geol. Soc. Am. 88, 857–868. https://doi.org/10.1130/0016-7606(1977)88<857:STADAR>2.0.CO;2

Xue, Z., He, R., Liu, J.P., Warner, J.C., 2012. Modeling transport and deposition of the Mekong River sediment. Cont. Shelf Res. 37, 66–78. https://doi.org/10.1016/j.csr.2012.02.010

Zhang, Q., Hirsch, R.M., Ball, W.P., 2016. Long-Term Changes in Sediment and Nutrient Delivery from Conowingo Dam to Chesapeake Bay: Effects of Reservoir Sedimentation. Environ. Sci. Technol. 50, 1877–1886. https://doi.org/10.1021/acs.est.5b04073